Chapter 11
Three-Body Problem

11.1 The N-Body Problem

11.1.1 Integrals of Motion

In Chap. 7, we have looked at two point masses that were moving under their mutual gravitational influence. Formally speaking we were dealing with two bodies each with six degrees of freedom (three position vector components and three velocity vector components). To describe their motion, in total 12 quantities had to be determined, specified by six coupled equations of motion of second order (see Eq. (7.1.14)) or 12 coupled equations of motion of first order:

$$\dot{\boldsymbol{v}}_1 = +\frac{Gm_2}{|\boldsymbol{r}_1 - \boldsymbol{r}_2|^3}(\boldsymbol{r}_1 - \boldsymbol{r}_2), \quad \boldsymbol{v}_1 = \dot{\boldsymbol{r}}_1$$
$$\dot{\boldsymbol{v}}_2 = -\frac{Gm_1}{|\boldsymbol{r}_1 - \boldsymbol{r}_2|^3}(\boldsymbol{r}_1 - \boldsymbol{r}_2), \quad \boldsymbol{v}_2 = \dot{\boldsymbol{r}}_2$$

By transforming the origin of the reference system into the center of mass of the two bodies (see Sect. 7.1.5) we were able to split the differential equations into two independent sets with three coupled equations of second degree each, namely $\ddot{\boldsymbol{r}} = -\mu\boldsymbol{r}/r^3$ and $\ddot{\boldsymbol{r}}_{CM} = 0$. We succeeded to directly integrate them, thus finding unambiguous analytical solutions.

A world with just two bodies is too idealistic in most cases. The motion of the Moon, for example, which circles the Earth, and at the same time is subject to the influence of the Sun, cannot be described adequately by just a two-body system. For these three bodies and for the general case of n bodies, one has to go back to the $6n$ coupled differential equations of first order, analogous to the above, which describe the acceleration and velocity of each body under the gravitational forces of all other bodies. The specific motion of these bodies is determined by the $6n$ quantities $(\boldsymbol{r}_1, \boldsymbol{v}_1), (\boldsymbol{r}_2, \boldsymbol{v}_2), \ldots, (\boldsymbol{r}_n, \boldsymbol{v}_n)$, which follow from integrating the

U. Walter, *Astronautics*, https://doi.org/10.1007/978-3-319-74373-8_11

differential equations. Their motion and hence the $(\boldsymbol{r}_1, \boldsymbol{v}_1)$, $(\boldsymbol{r}_2, \boldsymbol{v}_2), \ldots, (\boldsymbol{r}_n, \boldsymbol{v}_n)$ is, however, restricted due to the earlier discussed conservation laws. Mathematically, the conservation laws are 10 constraint equations for these $6n$ quantities, namely

- Six (i.e., 2×3) equations for the conservation of momentum of the center of mass (corresponds to the non-accelerated motion of the center of mass vector or equivalently to the initial values $\boldsymbol{v}_0$ and $\boldsymbol{r}_0$ of the center of mass, see Eq. (7.1.18).
- Three equations for the conservation of the total angular momentum.
- One equation for total energy conservation.

Each constraint equation defines a conserved quantity—a so-called "integral of motion" (here "integral" means a quantity that is independent of the motion and thus constant). So in essence there are $6n - 10$ degrees of freedom, which entails that $6n - 10$ quantities remain to be determined. Already in 1896 the French mathematician and physicist Henri Poincaré showed that for the general n-body problem (i.e., $n \geq 3$ bodies with arbitrary masses and arbitrary initial conditions), there cannot exist any further algebraic integrals of motion. So the general n-body problem is analytically not integrable, and thus cannot be solved analytically. Because in general the effective gravitational force on a body is no longer central, its trajectory is non-periodic, and because energy conservation applies to the entirety of bodies, a single body might gain or loose energy, such that even unbounded solutions may exist (see Sect. 11.1.2).

The n-body problem might not be solved analytically, but it is possible to solve it by other means. One possibility is to approximate the solution by convergent function series expansion. This mathematical method is rather complex, so we do not want to go into details here. We just mention that the expansion Eqs. (7.4.19) are function series expansions of the solution to Kepler's Equation (7.4.15) and Eq. (7.4.14) for elliptic orbits. In addition, with today's computers it is quite simple to get point-by-point solutions with arbitrary accuracies by solving the differential equations numerically for instance by Cowell's method described in Sect. 12.2.4. Despite the superior numerical capabilities, which today are exclusively applied for specific space missions, also the so-called patched-conics method, which we already got to know in Sect. 9.1, is regularly used to solve n-body problems by approximation. This method is used for interplanetary flights to gain preliminary insight into possible trajectories, which is indispensable to handle the complex calculation models of a detailed mission design.

11.1.2 Stability of an N-Body System

The basic reason why we are in general not able to analytically describe the orbits of n interacting bodies is that the energy and angular momentum of each single body are not conserved, but only those of the total system. This implies that any body may gain or lose energy and angular momentum in a random way by

gravitational interaction between the bodies. In this section we want to explore the stability of an n-body system and its conditions, i.e. the question whether a body may gain or lose energy indefinitely and thus is able to escape the system. In such a case we would call the system unstable.

Condition of System Instability
In a system with n bodies, $i = 1, \ldots, n$, having masses m_i and orbit radii r_i measured relative to the common barycenter consider the function

$$I := \sum_{i=1}^{n} m_i r_i^2 \quad \textbf{polar moment of inertia}$$

By construction I is always positive and also finite for bounded orbits. It becomes infinite if one or more of the n bodies escapes from the system. Therefore I may be considered as a good indicator for the stability of an n-body system. In this system we have for the total kinetic and total potential energy

$$E_{pot}(t) = -\sum_i \frac{\mu m_i}{r_i} \qquad \text{total potential energy of the system}$$

$$E_{kin}(t) = \frac{1}{2}\sum_i m_i \dot{r}_i^2 \qquad \text{total kinetic energy of the system}$$

$$E_{tot} = E_{kin} + E_{pot} = const \qquad \text{total energy of the system}$$

with μ the relevant gravitational parameter of the system. We now differentiate I twice and find

$$\ddot{I} = 2\sum_i m_i\left(\dot{r}_i^2 + r_i\ddot{r}_i\right)$$

With (see Eq. (7.1.5))

$$\sum_i m_i r_i \ddot{r}_i = \sum_i r_i F_i = -\sum_i r_i \frac{\partial}{\partial r_i} E_{pot} = -\sum_i \frac{\mu m_i}{r_i} = E_{pot}$$

we finally obtain

$$\ddot{I}(t) = 4E_{kin} + 2E_{pot} = 2E_{kin} + 2E_{tot} \tag{11.1.1}$$

Per definition E_{kin} is positive, while E_{tot} might be positive or negative. If $E_{tot} > -E_{kin}(t)$ for all times then from Eq. (11.1.1) it follows that $\ddot{I}(t) > 0$ and hence $I \to \infty$. This implies that at least one $r_i \to \infty$, meaning that at least one body escapes the system, or the entire system coherently disintegrates. On the other hand,

if the n-body system is stable then $E_{tot} < -E_{kin}$ must hold. Observe, however, that the reverse conclusion "$E_{tot} < -E_{kin} \rightarrow$ no body escapes the system", does not hold.

Virial Theorem

We will now prove that the virial theorem (7.3.20) also holds for the total kinetic and potential energy of an n-body system, regardless whether it is bounded or unbounded. In preparation for the proof, we formerly integrate Eq. (11.1.1)

$$\dot{I} = 4 \int_0^t E_{kin} \cdot dt' + 2 \int_0^t E_{pot} \cdot dt' + \dot{I}_0$$

We now let $t \rightarrow \infty$ and define P to be the longest period of all bounded bodies in the system. Thus we have with the time average of the system energies

$$\langle E \rangle := \frac{1}{P} \int_0^P E \cdot dt$$

$$\dot{I} = 4\langle E_{kin} \rangle t + 2\langle E_{pot} \rangle t + \dot{I}_0$$

or

$$\frac{1}{2}\dot{I}/t = 2\langle E_{kin} \rangle + \langle E_{pot} \rangle + \dot{I}_0/t$$

Hence

$$\frac{1}{2} \lim_{t \rightarrow \infty} \dot{I}/t = 2\langle E_{kin} \rangle + \langle E_{pot} \rangle$$

Applying l'Hôpital's rule $\lim_{t \rightarrow \infty} (\dot{I}/t) = 2 \lim_{t \rightarrow \infty} (I/t^2)$ we finally arrive at the result

$$2\langle E_{kin} \rangle + \langle E_{pot} \rangle = \lim_{t \rightarrow \infty} (I/t^2)$$

The term on the right hand side determines whether the system is bounded or not. As discussed above, as long as all bodies in the system stay bounded, $I < \infty$, and hence $\lim_{t \rightarrow \infty} (I/t^2) = 0$. So, for a bounded system and for times much longer than the longest body period we get the virial theorem

$$\boxed{\langle E_{pot} \rangle = -2\langle E_{kin} \rangle} \quad \textbf{virial theorem} \text{ for } \textbf{bounded} \text{ systems} \qquad (11.1.2)$$

Now let's consider an unbounded system, in which one or many bodies recede asymptotically to infinite distance from the barycenter (c.f. Pollard (1976, p. 67ff)).

At infinite distances the system can be considered as a single total point mass. Thus the motion of the detaching body becomes that of a 2-body system. From Eq. (7.4.28) we know that this is an asymptotic hyperbolic trajectory of the form

$$r(t) = v_\infty t + O(\ln\, t) + const \quad @\ t \to \infty$$

where $v_\infty = \sqrt{-\mu/a}$ is the hyperbolic excess velocity (see Sect. 7.4.3). Hence we get for an escaping body with mass m

$$\lim_{t\to\infty} \frac{I}{t^2} = \lim_{t\to\infty} \frac{mr^2}{t^2} = mv_\infty^2$$

The virial theorem for an unbounded system with j bodies having escaped the system and for times much longer than the longest body period in the bounded system part therefore reads

$$\boxed{2\langle E_{kin}\rangle + \langle E_{pot}\rangle = \sum_{i=1}^{j} m_i v_{i,\infty}^2} \quad \textbf{virial theorem} \text{ for } \textbf{unbounded} \text{ systems} \tag{11.1.3}$$

This result is conclusive because the left hand side of the equation is twice the energy of the remaining bounded bodies, while the right hand side is twice the hyperbolic excess kinetic energy of the escaped bodies.

System Collapse

We now wonder whether a n-body system might collapse. To find a stability condition we study the absolute value of the total angular momentum

$$L = \left|\sum_i m_i \boldsymbol{r}_i \times \boldsymbol{v}_i\right| \le \sum_i m_i |\boldsymbol{r}_i \times \boldsymbol{v}_i| \le \sum_i m_i r_i v_i = \sum_i (\sqrt{m_i} r_i)(\sqrt{m_i} v_i)$$

By setting $a_i := r_i\sqrt{m_i}$ and $b_i := v_i\sqrt{m_i}$ and applying Cauchy's inequality

$$\left(\sum\nolimits_i a_i b_i\right)^2 \le \left(\sum\nolimits_i a_i^2\right)\left(\sum\nolimits_i b_i^2\right)$$

we obtain

$$L^2 \le \sum_i m_i r_i^2 \sum_i m_i v_i^2 = 2I \cdot E_{kin}$$

which delivers Sundman's inequality

$$E_{kin} \ge \frac{L^2}{2I} \quad \textbf{Sundman's inequality} \tag{11.1.4}$$

From Sundman's inequality follows directly.

Sundman's theorem
A many-body system made up of point masses (in fact any planetary system) that at any point in time has a finite kinetic energy and total angular momentum, i.e. $I \neq 0$, can never fully collapse.

Since for our solar system today $E_{kin} > 0$, $L > 0$, it will never fully collapse. Good to know. Note, however, that partial collapses in the form of binary collisions and collisions between up to $n - 1$ bodies are possible.

Caution is in place with accepting Sundman's theorem for describing the long-term fate of our solar system and any stellar system in general. The planets will not endlessly circulate the Sun. In about 5 billion years our Sun will expand, become a so-called Red Giant, and swallow successively first Mercury, then Venus und finally even Earth. In addition, the solar wind made up of mostly protons constantly sweeps out of our solar system, thus loosing mass and with it angular momentum and kinetic energy. By the same token solar radiation makes the Sun loose energy. Finally gravitational waves caused by the orbiting planets make their orbits shrink over very long time scales. And, last but not least, there is a high probability that our solar system may collide with another star system, by which either system is broken up or at least some of the planets are slung out of these systems. So the key point about the fate of our solar system is that it is not a closed system, which revolves forever, but its fate is determined by its interactions with the universe through radiation and by collisions.

11.1.3 N-Body Choreographies

There are many-body systems, so-called *n-body choreographies*, that show a synchronous and concerted motion of all bodies under very special conditions. One condition is that all masses are exactly the same. The other is that they have to have very special initial positions and velocities. In an *n*-body choreography all bodies move either on a single winding two-dimensional orbit or they move on several winding orbits, each of which may not be flat, thus these orbits cover three-dimensional space and are generally intertwined.

It was only in 2000 that a solution was found where three bodies revolve around each other in an orbit of the form of a figure 8 (see Fig. 11.1). In contrast to many other similar, symmetrical, co-orbital orbits with more than three bodies (see Figs. 11.2 and 11.3), which are not stable, this figure-eight orbit is dynamically stable. The so-called stability domain, that is the range of admissible deviations

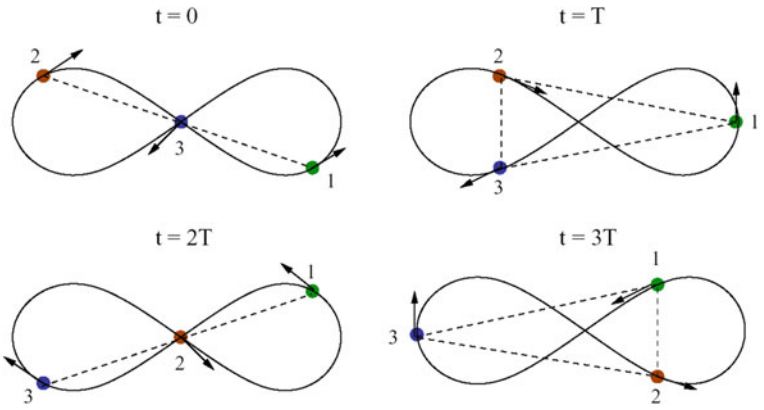

Fig. 11.1 The figure-eight orbit. A stable co-orbital motion of three masses on an 8-shaped orbit at different time intervals. *Credit* A. Chenciner and R. Montgomery

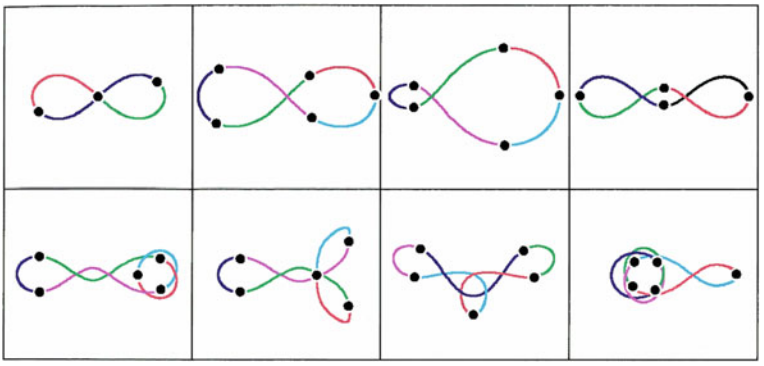

Fig. 11.2 Planar n-body choreographies of three to five masses. Colors indicate the orbits of the masses from their current position to their next symmetrical position. *Credit* Robert Jenkins and Carles Simó

from the ideal orbit or mass, however, is so small that numerical simulations predict only 1–100 instances of figure-eight orbits in the observable universe.

See www.maths.manchester.ac.uk/∼jm/Choreographies/ for many more animations on n-body choreographies.

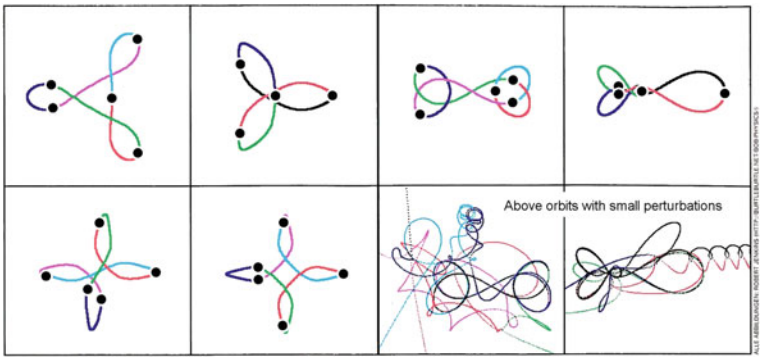

Fig. 11.3 More planar n-body choreographies of four and five masses. Colors indicate the orbits of the masses from their current position to their next symmetrical position. *Credit* Robert Jenkins and Carles Simó

11.2 Synchronous 3-Body Orbits

In this section we examine two special 3-body choreographies with possibly different masses, and which have already been known for 250 years. The property of the general *n*-body problem, that the trajectories of the bodies are non-periodic and may even be unbounded, does not hold for two other special cases of 3-body systems where all bodies always display a constant motion-pattern with either synchronous unbounded or bounded periodic trajectories:

1. *Collinear configuration*—three arbitrary masses move synchronously in a linear configuration with fixed relative distances on Keplerian orbits (ellipses, parabolas, or hyperbolas).
2. *Equilateral configuration*—three arbitrary masses move synchronously in an equilateral triangle configuration with fixed relative distances on coplanar Keplerian orbits (ellipses, parabolas, or hyperbolas).

We shall now look at these two special constant motion-patterns.

11.2.1 Collinear Configuration

Already in 1765 the Swiss mathematician Leonhard Euler showed that if the three bodies with arbitrary masses adopt certain positions on a straight line—called *collinear libration points,* a.k.a. *Eulerian points*—their joint motion can be described as a rotation of this straight line where their mutual distances change such that the distance ratios, and hence the entire configuration, remain constant

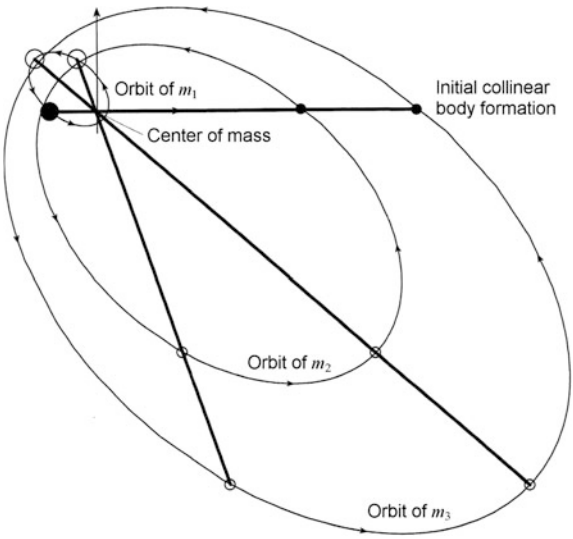

Fig. 11.4 Dynamics of the collinear masses configuration with $m_1' = 1/10$ Earth mass, $m_2' =$ Moon mass, $m_3' = 1/2$ Moon mass

(see Fig. 11.4). Because Euler's collinear configuration is of high relevance for the R3BP, we will take a closer look at its mathematical description.

Let m_1', m_2', m_3' be three collinear masses of arbitrary size, where, without loss of generality, the mass labeled m_2' is located between the other two, m_1' and m_3', and $m_1' \geq m_3'$. With regard to their common center of mass their relative distances and coordination can therefore described by the two constants α, β relating their position vectors $\boldsymbol{r}_i$, $i = 1, 2, 3$ as

$$\begin{aligned} \boldsymbol{r}_3 &= \alpha \boldsymbol{r}_2, \quad \alpha > 1 \\ \boldsymbol{r}_1 &= \beta \boldsymbol{r}_2, \quad \beta < 0 \end{aligned} \tag{11.2.1}$$

With this we get from the center-of-mass equation (cf. Eq. (7.1.17)) $\sum_i m_i' \boldsymbol{r}_i = 0$

$$\beta m_1' + m_2' + \alpha m_3' = 0 \tag{11.2.2}$$

Given this, it can be shown (see Guthmann (2000)) that in an inertial reference frame with origin in their common center of mass each rotating mass obeys one of the following three interrelated equations of motion

$$\ddot{\boldsymbol{r}}_i + \frac{\mu_i}{r_i^3} \boldsymbol{r}_i = 0, \quad i = 1, 2, 3 \tag{11.2.3}$$

with

$$\begin{aligned}\frac{\mu_1}{G} &= \frac{\beta^2 m_2'}{(1-\beta)^2} + \frac{\beta^2 m_3'}{(\alpha-\beta)^2} \\ \frac{\mu_2}{G} &= -\frac{m_3'}{(\alpha-1)^2} + \frac{m_1'}{(1-\beta)^2} \\ \frac{\mu_3}{G} &= \frac{\alpha^2 m_2'}{(\alpha-1)^2} + \frac{\alpha^2 m_1'}{(\alpha-\beta)^2}\end{aligned} \tag{11.2.4}$$

It can be shown (Exercise, Problem 11.2, cf. Guthmann (2000)) that α is the unequivocal *positive* root and β the unequivocal *negative* root of

$$\begin{aligned}\mu_3 &= \alpha^3 \mu_2 \\ \mu_1 &= -\beta^3 \mu_2\end{aligned} \tag{11.2.5}$$

Because according to Eq. (11.2.3) each mass is subject to a central Newtonian force, the orbits must be Keplerian orbits (conic sections). With a_i being their semi-major axes it follows immediately from Eqs. (11.2.1) and (11.2.2) that

$$\sqrt{\frac{\mu_i}{a_i^3}} = n = const \tag{11.2.6}$$

The three orbits therefore have the same mean motion and thus the same orbital frequency and hence orbital period.

Initial Conditions
Let us assume that we start the motion such that the three masses are in a collinar configuration with α and β given by Eq. (11.2.5), i.e., all three Keplerian orbits have a common true anomaly θ. In addition, if we choose the initial velocities of each mass to be

1. proportional in magnitude to its distance to the center of mass, and
2. their velocity vectors form equal angles with their corresponding radial position vectors

From Eqs. (11.2.1) and (11.2.6) follows that $r_1/a_1 = r_2/a_2 = r_3/a_3$. This implies with Eq. (7.3.5) that

$$e_1 = e_2 = e_3 =: e \tag{11.2.7}$$

Given these results, all three Keplerian orbits obey

$$r_i = \frac{a_i(1-e^2)}{1+e\,\cos\theta} \tag{11.2.8}$$

Rotation Dynamics

We now show that under the said initial conditions the motion of the masses conserves their collinearity. To do so we prove that the orbital frequency of each of the three bodies is the same at any time. With $e_i = e$ and Eq. (7.2.7) we get

$$\omega_i = \frac{h_i}{r_i^2} = \frac{\sqrt{\mu_i a_i (1-e^2)}}{r_i^2}$$

With Eqs. (11.2.1) and (11.2.5) we find

$$\omega_3 = \frac{\sqrt{\mu_3 a_3 (1-e^2)}}{r_3^2} = \frac{\sqrt{\alpha^3 \mu_2 \alpha a_2 (1-e^2)}}{\alpha^2 r_2^2} = \omega_2$$

and

$$\omega_1 = \frac{\sqrt{\mu_1 a_1 (1-e^2)}}{r_1^2} = \frac{\sqrt{-\beta^3 \mu_2 (-\beta) a_2 (1-e^2)}}{\beta^2 r_2^2} = \omega_2$$

This proves that all three orbits have the equal instantaneous orbital frequency

$$\omega(\theta) = \frac{\sqrt{\mu_i a_i (1-e^2)}}{r_i^2} = \sqrt{\frac{\mu_i}{a_i}} \frac{(1+e\,\cos\theta)^2}{a_i (1-e^2)^{3/2}} = \frac{2\pi}{T} \frac{(1+e\,\cos\theta)^2}{(1-e^2)^{3/2}} \qquad (11.2.9)$$

> The collinear masses rotate on a straight line, with variable absolute distances, but constant relative distances between the masses—like a rotating rubber band.

As an example, Fig. 11.5 shows the dynamics of three collinear, rotating masses with $m_1' = 1/10$ Earth mass, $m_2' =$ Moon mass, $m_3' = 1/2$ Moon mass. The relative distances on the rotating configuration line are obviously retained, and the individual masses co-rotate on ellipses with a common line of apsides, and with the focus in the joint center of mass.

One may be surprised that the motion of the masses is indeed on a straight line, as this seems to contradict $n = \sqrt{\mu/a^3}$, which infers that the mean orbital motion

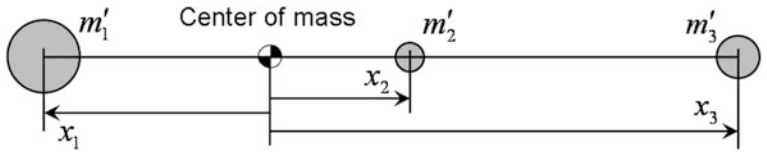

Fig. 11.5 Definitions for the collinear configuration with arbitrary masses, where the mass in the middle is denoted as m_2' and without loss of generality $m_1' \geq m_3'$

n of a mass is different for different semi-major axes. But one has to consider that according to Eq. (11.2.4) every orbit has a different μ_i from which Eq. (11.2.6), $n = \sqrt{\mu_i/a_i^3}$ follows.

Reference Frame

Because the points are collinear and the distance ratios of the masses are fixed by the constants α and β, we choose the configuration line as our co-rotating coordinate x-axis so that the masses are located at positions $\boldsymbol{r}_i = (x_i, 0, 0)$ (see Fig. 11.5). Then by the above definition, $x_3 = \alpha x_2$ and $x_1 = \beta x_2$. The collinear configuration can be characterized by the configuration parameter χ, which is defined in terms of the relative distances

$$\begin{aligned} x_{12} &:= x_2 - x_1 \\ x_{13} &:= x_3 - x_1 = (1+\chi)x_{12} \\ x_{23} &:= x_3 - x_2 = \chi x_{12} \end{aligned} \tag{11.2.10}$$

$$\chi := \frac{x_{23}}{x_{12}} = \frac{x_3 - x_2}{x_2 - x_1} = \frac{\alpha - 1}{1 - \beta} > 0 \tag{11.2.11}$$

With χ we relate the distances of the masses to the reference distance x_{12}, which may be chosen freely. The parameter χ is solely determined by the three masses, the details of which will be studied in a moment.

Lagrange's Quintic Equation

We now want to determine the constant, relative positions of the masses on the line, as described by χ, from the given masses. Because the three masses are configuration-invariant on a straight line we need not to solve the equation of motion, but it suffices to derive a conditional equation for χ determined by the three masses. Equation (11.2.11) results in

$$\alpha - \beta = (1+\chi)(1-\beta) = \frac{1+\chi}{\chi}(\alpha - 1)$$

With this and Eq. (11.2.4) we can rewrite the conditional Eq. (11.2.5), $\mu_3 = \alpha^3 \mu_2$, as

$$\alpha\left[-\frac{m_3'}{(\alpha-1)^2} + \frac{m_1'}{(1-\beta)^2}\right] = \frac{m_2'}{(\alpha-1)^2} + \frac{m_1'}{(\alpha-\beta)^2}$$

and

$$\alpha\left(\chi^2 m_1' - m_3'\right) = m_2' + m_1' \frac{\chi^2}{(1+\chi)^2}$$

On the other hand, from the center-of-mass equation $\beta m_1' + m_2' + \alpha m_3' = 0$ and the above follows that

$$1 - \beta = \frac{m_1' + m_2' + \alpha m_3'}{m_1'} = \frac{\alpha - 1}{\chi}$$

Hence

$$\alpha = \frac{m_1' + \chi(m_1' + m_2')}{m_1' - \chi m_3'}$$

Inserting this into the above equation leads to

$$\frac{m_1' + \chi(m_1' + m_2')}{m_1' - \chi m_3'} \left(\chi^2 m_1' - m_3'\right) = m_2' + m_1' \frac{\chi^2}{(1+\chi)^2} \tag{11.2.12}$$

After some basic algebra, this equation can be transformed into **Lagrange's quintic equation**

$$\begin{aligned}&(m_1' + m_2')\chi^5 + (3m_1' + 2m_2')\chi^4 + (3m_1' + m_2')\chi^3 \\ &\quad - (m_2' + 3m_3')\chi^2 - (2m_2' + 3m_3')\chi - (m_2' + m_3') = 0\end{aligned} \tag{11.2.13}$$

for the given masses m_1', m_2' and m_3', where m_2' is located in the middle. The single positive root χ of Lagrange's quintic equation determines via the given reference distance x_{12} and by means of Eq. (11.2.10) all the other distances.

Note 1 *Because the coefficients of the powers of χ change sign only once, from Descartes' rule of signs follows that there is only a single positive root of Lagrange's quintic equation.*

Note 2 *Equation (11.2.13) holds for any type of collinear Keplerian orbit that obeys Eq. (11.2.3), be it bounded or unbounded.*

The synchronous motion of the collinear configuration only takes place if there are no perturbations. In the presence of even the tiniest perturbation of the configuration the collinear configuration is always *unstable*, even in the R3BP limit: The masses then will run away from this configuration.

Circular Orbits

If the initial conditions are such that the three bodies move on circular orbits, then the absolute distances, and in particular x_{12}, are even constant. The uniform period for these circular orbits turns out (exercise, Problem 11.3) to be

$$\omega = n = \frac{2\pi}{T} = \sqrt{\frac{\mu}{x_{12}^3}\frac{m_1'\chi^2 - m_3'}{m_1' - m_3'\chi}} = \sqrt{\frac{\mu_i}{x_i^3}} = const \tag{11.2.14}$$

with

$$\mu = GM = G\left(m_1' + m_2' + m_3'\right)$$

In this case Euler's collinear configuration is not only configuration-invariant, but also form-invariant. The fixed positions in the co-rotating synodic reference frame are called *stationary points*.

11.2.2 Equilateral Configuration

We are seeking for all three-body configurations, where the three co-moving masses take up a fixed configuration. It can be shown that other than the collinear configuration there can exist only one more such configuration, which was found in 1772 by the French mathematician Joseph Lagrange and sometimes named after him. The results will merely be summarized here without proof. Lagrange's configuration is a configuration of three bodies with arbitrary masses m_1, m_2, m_3, which without loss of generality we order by their mass quantity, $m_3 < m_2 < m_1$. They show an equilateral triangular formation and obey one of the corresponding three Newton's gravitational EoM

$$\ddot{\boldsymbol{r}}_i + \frac{\mu_i}{r_i^3}\boldsymbol{r}_i = 0 \quad \text{for} \quad i = 1, 2, 3$$

with

$$\begin{aligned} \mu_1 &= \tfrac{G}{M^2}\left(m_2^2 + m_3^2 + m_2 m_3\right)^{3/2} \\ \mu_2 &= \tfrac{G}{M^2}\left(m_1^2 + m_3^2 + m_1 m_3\right)^{3/2} \\ \mu_3 &= \tfrac{G}{M^2}\left(m_1^2 + m_2^2 + m_1 m_2\right)^{3/2} \end{aligned} \tag{11.2.15}$$

and

$$M = m_1 + m_2 + m_3$$

If the initial conditions for each mass are such that

1. The net resultant force on a mass is a position vector through the system center of mass.
2. The velocity of a mass is proportional in magnitude to its distance to the center of mass.
3. The velocity vectors form equal angles with their corresponding radial position vectors.

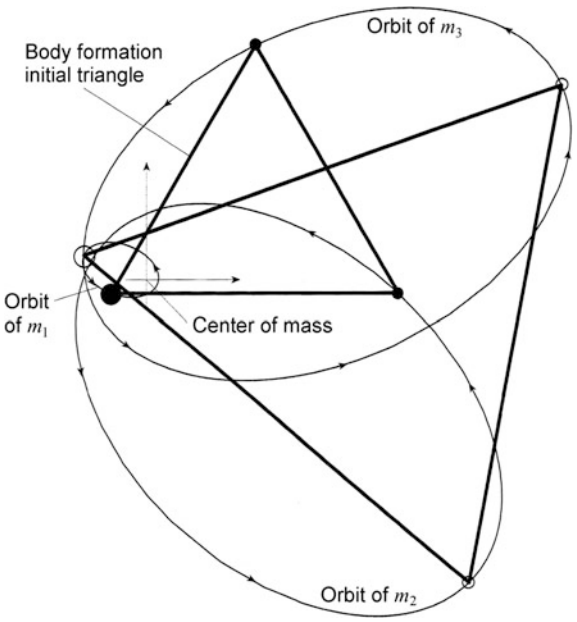

Fig. 11.6 Dynamics of an equilateral configuration with elliptic orbits

it can be shown that the equilateral configuration, just like the collinear configuration, does not change its symmetry, but merely is stretched in space, that is, its distances change, but their ratios remain constant (see Fig. 11.6). We state this property as follows:

> The equilateral configuration while rotating continuously changes its size—it is "breathing".

If the total energy of the system is negative, zero, or positive, this results in bounded ellipses (or circles), or unbounded parabolas or hyperbolas, revolving around a common center of mass. The size of their semi-axis depends on the size of the individual mass. Figure 11.6 shows a bounded system with the masses: 1/10 Earth mass, Moon mass, and half the mass of the Moon.

Though Lagrange's equilateral configuration has a remarkable symmetry, it is generally unstable: it disintegrates after a certain period of time. It is only dynamically stable in the limit of a restricted three-body configuration (see next section) when one primary mass is significantly bigger than the other (see Eq. (11.5.12)).

Circular Orbits

If the initial conditions are such that the three bodies move in circles, then, like the collinear configuration, the equilateral configuration is not only configuration-invariant,

but also form-invariant. It can be shown (exercise, Problem 11.4) that in this case the orbital frequency is given as

$$\omega = n = \frac{2\pi}{T} = \sqrt{\frac{\mu_i}{r_i^3}} = \sqrt{\frac{\mu}{r_{ij}^3}} = const \tag{11.2.16}$$

with the distance between the bodies

$$r_{ij} := r_{12} = r_{23} = r_{13}$$

and

$$\mu = GM = G(m_1 + m_2 + m_3)$$

11.3 Restricted Three-Body Problem

The general collinear and equilateral configurations are quite academic cases. From a practical point of view, only the special case of the *restricted three-body problem* (R3BP) plays a role. Here one of the three masses, denoted m, e.g. a spacecraft, is negligibly small compared with the other two, the so-called *primary bodies*. As an example the primaries might be Earth–Moon or Sun–Earth. As we have seen before, the collinear and equilateral configurations hold for any masses m_1, m_2, m_3 and therefore also for the R3BP.

Without restriction to generality we label the lighter of the two primaries, the so-called **minor primary**, as m_2, and the **major primary** as m_1, that is

$$m \ll m_2 < m_1$$

In addition and for later convenience we normalize the masses of the two primaries by their total mass $M = m_1 + m_2$

$$\mu := \frac{m_2}{m_1 + m_2} < \frac{1}{2} \quad \text{reduced minor primary mass} \tag{11.3.1}$$

$$1 - \mu = \frac{m_1}{m_1 + m_2} < 1 \quad \text{reduced major primary mass}$$

The two primary masses are rotating in general on elliptic orbits with varying angular velocity $\omega(t)$ and varying mutual distance $d(t)$ about their barycenter.

Euler defined the R3BP in 1772, after he had already discovered in 1765 the collinear equilibrium points, the results of which also apply to the R3BP. Also in 1772 Lagrange discovered all five equilibrium points in the R3BP including the two equilateral equilibrium points. Ever since then, the collinear equilibrium points of

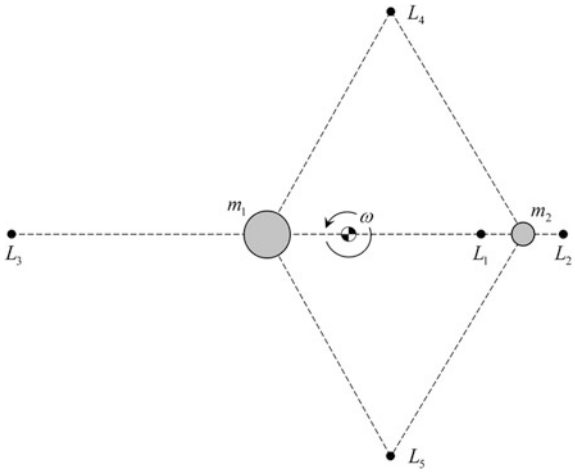

Fig. 11.7 Location of the collinear points L_1 to L_3 and equilateral points L_4 and L_5 in the R3BP

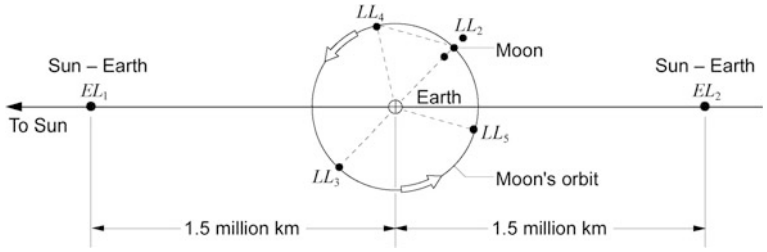

Fig. 11.8 Libration points in the vicinity of Earth

mass m in the R3BP are also known as *Eulerian points* L_1, L_2, L_3, and the equilateral equilibrium points are also known as *Lagrangian points* L_4 and L_5 (see Figs. 11.7 and 11.8). All five points together are the so-called *libration points*, but quite frequently and confusingly they are also called *Lagrangian points*. We evade this equivocality by labeling them as (Euler's) collinear libration points and (Lagrange's) equilateral libration points.

Note *In literature the libration points are not uniquely labeled. In this book we adopt the most frequent labeling:* L_1 *is the point between the two primaries,* L_2 *the point beyond the minor primary, and* L_3 *the point opposite to the minor primary. One often finds a reverse labeling of* L_1 *and* L_2*. Unfortunately, an inconsistent labeling is used also for the equilateral libration points. As usual we call* L_4 *the leading and* L_5 *the trailing equilateral libration point with respect to motion of the minor primary* m_2 *(But see for instance Wiesel (1997) and Roy (2005) for a reverse labeling.).*

Terminology In short notation Sun-Earth libration points are called EL, e.g. Sun-Earth L_1 is EL_1. Earth–Moon (lunar) libration points are called LL, e.g. Earth-Moon L_2 is LL_2 (see Fig. 11.8).

We now take a look at the characteristics of the libration points.

11.3.1 Collinear Libration Points

First of all, we introduce appropriate distance variables: Let Δ_i be the distance from a collinear libration point L_i to the center of the major primary body normalized to the distance between the two primary bodies. According to Fig. 11.4 and Eq. (11.2.10) the following holds for these normalized distances

$$\begin{aligned} \Delta_3 &:= \frac{x_{23}}{x_{12}} = \chi \\ \Delta_2 &:= \frac{x_{13}}{x_{12}} = 1+\chi \\ \Delta_1 &:= \frac{x_{12}}{x_{13}} = \frac{1}{1+\chi} \end{aligned} \tag{11.3.2}$$

As our considerations in Sect. 11.2.2 were valid for collinear configurations with any masses, we get from Eq. (11.2.12) for $m_3' = m \approx 0$ the following conditional equation of the configuration parameter χ for the collinear points L_2 and L_3

$$m_1' + \chi\left(m_1' + m_2'\right) = \frac{m_2'}{\chi^2} + \frac{m_1'}{(1+\chi)^2} \tag{11.3.3}$$

We recall that the primed masses are labeled according to their position (m_2' is in the middle, see Fig. 11.5), and unprimed masses according to their masses, $m \ll m_2 < m_1$.

L_3 point
Now, if $m_2' > m_1'$, then $m_2' = m_1$, $m_1' = m_2$, and $m_3' = m$ is located at the L_3 point. In this case, we get from Eq. (11.3.1)

$$\mu = \frac{m_2}{m_1+m_2} = \frac{m_1'}{m_2'+m_1'} = \frac{1}{1+m_2'/m_1'}$$

from which follows

$$\frac{m_2'}{m_1'} = \frac{1-\mu}{\mu}$$

With this and with Eq. (11.3.2a) we get from Eq. (11.3.3) the conditional equation for Δ_3

$$\Delta_3 + \mu = \frac{\mu}{(1+\Delta_3)^2} + \frac{1-\mu}{\Delta_3^2} \quad @\ \boldsymbol{L_3}\ \textbf{point} \tag{11.3.4}$$

***L_2* point**

If $m_1' > m_2'$, then $m_2' = m_2$, $m_1' = m_1$, and $m_3' = m$ is located at the L_2 point near m_2. In this case, we get

$$\mu = \frac{m_2}{m_1 + m_2} = \frac{m_2'}{m_1' + m_2'} = \frac{1}{1 + m_1'/m_2'}$$

from which follows

$$\frac{m_1'}{m_2'} = \frac{1-\mu}{\mu}$$

With this and with Eq. (11.3.2b) we get from Eq. (11.3.3) the conditional equation for Δ_2

$$\Delta_2 - \mu = \frac{\mu}{(1-\Delta_2)^2} + \frac{1-\mu}{\Delta_2^2} \quad @\ \boldsymbol{L_2}\ \textbf{point} \tag{11.3.5}$$

***L_1* point**

Finally, if $m_1' > m_3'$ then $m_1' = m_1$, $m_3' = m_2$, and $m_2' = m \approx 0$ is located at the L_1 point near m_2. Because of Eq. (11.2.12), we get for the conditional equation of the configuration parameter χ

$$\chi^2 m_1' - m_3' = \frac{\chi^2}{(1+\chi)^3}\left(m_1' - \chi m_3'\right)$$

and

$$\mu = \frac{m_2}{m_1 + m_2} = \frac{m_3'}{m_1' + m_3'} = \frac{1}{1 + m_1'/m_3'}$$

from which follows

$$\frac{m_1'}{m_3'} = \frac{1-\mu}{\mu}$$

With this and Eq. (11.3.2c) we get as the conditional equation for Δ_1

$$\Delta_1 - \mu = -\frac{\mu}{(1-\Delta_1)^2} + \frac{1-\mu}{\Delta_1^2} \quad @\ \boldsymbol{L_1}\ \textbf{point} \tag{11.3.6}$$

Location of Collinear Libration Points

Since $\mu < 1$ the solutions of Eqs. (11.3.4)–(11.3.6) can be determined (exercise, Problem 11.5) by power series approximations (cf. Szebehely (1967, p.134ff))

$$\begin{aligned}
\Delta_1 &= 1 - \lambda + \frac{1}{3}\lambda^2 + \frac{1}{9}\lambda^3 - \frac{58}{81}\lambda^4 + \frac{11}{243}\lambda^5 + \frac{4}{9}\lambda^6 + \cdots < 1 \\
\Delta_2 &= 1 + \lambda + \frac{1}{3}\lambda^2 - \frac{1}{9}\lambda^3 + \frac{50}{81}\lambda^4 + \frac{43}{243}\lambda^5 - \frac{4}{9}\lambda^6 + \cdots > 1 \\
\Delta_3 &= 1 - \frac{7}{12}\mu - \frac{1127}{20736}\mu^3 - \cdots < 1
\end{aligned} \tag{11.3.7}$$

with

$$\lambda := \left(\frac{\mu}{3}\right)^{1/3} = \left(\frac{1}{3}\frac{m_2}{m_1+m_2}\right)^{1/3}$$

For the Sun–planet or planet–Moon systems $\mu \ll 1$ and hence Eq. (11.3.7) provides very good approximations. Only for the Earth–Moon system $\lambda = 0.159401$ is relatively big, leading to a correspondingly worse convergence. In Eq. (11.3.7), the collinear distances are given with regard to the distance between the two primary bodies. If both primary orbits are circular then the collinear libration points also have fixed distances relative to the center of mass. If their orbits are elliptic, their mutual distance changes, and with it also the absolute distance to the collinear libration points.

From a physical point of view the positions of the collinear libration points result from the sum of the gravitational forces from both primaries, plus the centrifugal force of its rotation around the center of mass. This is why, for example, the L_1 point is not located where the gravitational forces of m_1 and m_2 just cancel each other out, but further in the direction to the major primary, to balance the centrifugal force by a somewhat larger gravitational force.

11.3.2 Equilateral Libration Points

The two equilateral libration points are determined by the equilaterality property of the triangle m_1, m_2, m. That is,

$$\begin{aligned} \frac{\Delta x}{d} &= 0.5, \quad \frac{\Delta y}{d} = +\frac{\sqrt{3}}{2}, \quad \Delta_4 = \frac{\Delta x^2 + \Delta y^2}{d^2} = 1 \quad @\ L_4 \\ \frac{\Delta x}{d} &= 0.5, \quad \frac{\Delta y}{d} = -\frac{\sqrt{3}}{2}, \quad \Delta_5 = \frac{\Delta x^2 + \Delta y^2}{d^2} = 1 \quad @\ L_5 \end{aligned} \tag{11.3.8}$$

where Δy measures the distance perpendicular to the configuration line of the two primaries and d is their mutual distance.

Table 11.1 shows specific examples: the exact position of all libration points in the Earth–Moon system with $m_{Earth}/m_{Moon} = 81.30094$.

11.4 Circular Restricted Three-Body Problem

Up to now we have examined the R3BP where the test mass m is negligibly small compared to the other two primary masses m_1, m_2, which are rotating on elliptic orbits about their barycenter implying varying angular velocity ω and varying mutual distance d. We now assume that the initial conditions are such that their orbits are circular so that $d = const$ and hence according to Eq. (7.4.1)

$$\omega = n = \sqrt{\frac{G(m_1 + m_2)}{d^3}} = const$$

In this section we want to study the situation where the test mass is free to move with respect to the primary masses. This test mass, for instance, might be a Moon probe on a quite convoluted trajectory from Earth to the Moon. The determination

Table 11.1 Libration points in the Earth–Moon system

Libration points	$\Delta x/d$	$\Delta y/d$	C
L_1	0.849068	0	−1.6735
L_2	1.167830	0	−1.6649
L_3	0.992912	0	−1.5810
L_4	0.500000	0.866025	−1.5600
L_5	0.500000	−0.866025	−1.5600

Here Δx is the distance of a libration point to the Earth on the x-axis, which is the configuration line between Earth and Moon; Δy is the distance of a libration point to Earth perpendicular to the configuration line; and d the distance between Earth and Moon. C is the Jacobi constant (see Sect. 11.4.2) for $v = 0$

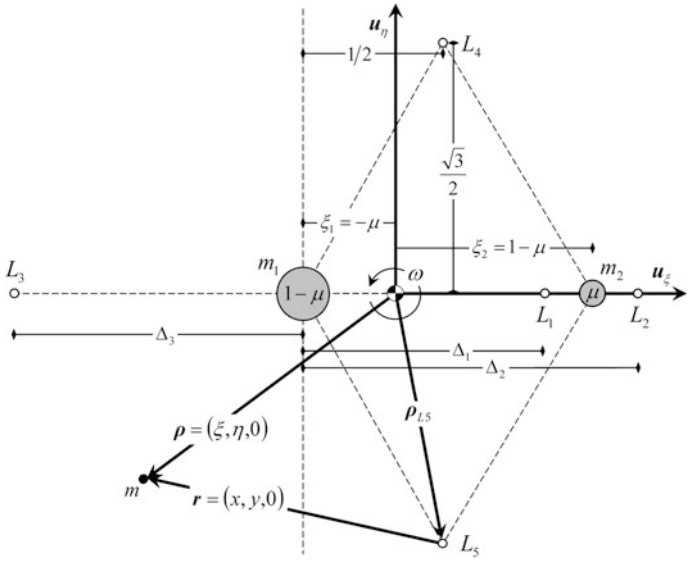

Fig. 11.9 Positions, distances, and vectors in the synodic reference frame of a CR3BP. Vector $\boldsymbol{r}$ as defined in Sect. 11.5.1

of the motion of the test mass between these circularly rotating primaries is called the *circular restricted three-body problem*, CR3BP.

The Synodic Reference Frame

To determine the trajectory of m we define the co-rotating (synodic) reference frame by the orthonormal axes $(\boldsymbol{u}_\xi, \boldsymbol{u}_\eta, \boldsymbol{u}_\zeta)$ (see Fig. 11.9) where $\boldsymbol{u}_\xi$ points from the barycenter to the minor primary m_2, $\boldsymbol{u}_\zeta$ points along the total angular momentum $\boldsymbol{h}$ being vertical to the common motion plane, and $\boldsymbol{u}_\eta$, lying in the plane of rotation and pointing to the half-plane where L_4 is located, completes the right-handed reference system. Within this synodic reference frame we define the normalized position vector to m as

$$\boldsymbol{\rho} := \xi \boldsymbol{u}_\xi + \eta \boldsymbol{u}_\eta + \zeta \boldsymbol{u}_\zeta = \boldsymbol{r}/d \tag{11.4.1}$$

where the coordinates ξ, η, ζ are the axis intercepts normalized by d and therefore dimensionless. Due to $m \approx 0$, the two primaries have the fixed positions $\boldsymbol{\rho}_i = (\xi_i, 0, 0)$ in this synodic reference frame with $\xi_2 - \xi_1 = 1$ following from the normalizing condition. With this relation and from the center-of-mass conditions (see Sect. 7.1.5) $(1-\mu)\xi_1 + \mu\xi_2 = 0$ we find that the minor primary with mass μ is located at $\xi_2 = 1-\mu$ while the bigger one with mass $1-\mu$ is at $\xi_1 = -\mu$. Hence

$$\boldsymbol{\rho}_i = (\xi_i, 0, 0) = \begin{pmatrix} -\mu & 0 & 0 \\ 1-\mu & 0 & 0 \end{pmatrix} \quad \left\{ \begin{array}{l} i = 1, \text{ major primary} \\ i = 2, \text{ minor primary} \end{array} \right\} \tag{11.4.2}$$

Therefore, the relative distances of m to the primaries are

$$\begin{aligned} \Delta\rho_1 &= |\boldsymbol{\rho} - \boldsymbol{\rho}_1| = \sqrt{(\xi+\mu)^2 + \eta^2 + \zeta^2} \\ \Delta\rho_2 &= |\boldsymbol{\rho} - \boldsymbol{\rho}_2| = \sqrt{[\xi-(1-\mu)]^2 + \eta^2 + \zeta^2} \end{aligned} \tag{11.4.3}$$

Thus, the gravitational potential for the test mass m can be rewritten as

$$\begin{aligned} U &= -\frac{Gm_1}{|\boldsymbol{r} - \boldsymbol{r}_1|} - \frac{Gm_2}{|\boldsymbol{r} - \boldsymbol{r}_2|} \\ &= -\frac{G(m_1+m_2)}{d}\left(\frac{1-\mu}{\Delta\rho_1} + \frac{\mu}{\Delta\rho_2}\right) =: d^2 n^2 U' \end{aligned} \tag{11.4.4}$$

with

$$U' = -\frac{1-\mu}{\Delta\rho_1} - \frac{\mu}{\Delta\rho_2}$$

11.4.1 Equation of Motion

Quite generally, the equation of motion is derived from Newton's second law of motion, Eq. (7.1.12). Due to $m \approx 0$ the barycenter of the three bodies is identical to the barycenter of the two primaries and hence the acting force stems by virtue of Eq. (7.1.5) from the gravitational potential U as

$$m\ddot{\boldsymbol{r}} = \boldsymbol{F} = -m\frac{\partial U}{\partial \boldsymbol{r}}$$

We cross over to the synodic reference frame by inserting Eqs. (11.4.1) and (11.4.4), which leads to

$$\ddot{\boldsymbol{\rho}} = -n^2 \frac{\partial U'}{\partial \boldsymbol{\rho}}$$

To study the motion in this non-inertial synodic reference frame rotating with a constant angular velocity $\boldsymbol{n} = (0, 0, n)$ we have to transform $\ddot{\boldsymbol{\rho}}$ according Eq. (7.2.2) as

$$\begin{aligned}\ddot{\boldsymbol{\rho}} &= \ddot{\boldsymbol{\rho}}|_{syn} + \overbrace{2\boldsymbol{n}\times\dot{\boldsymbol{\rho}}|_{syn}}^{Coriolis\ force} + \overbrace{\boldsymbol{n}\times(\boldsymbol{n}\times\boldsymbol{\rho})}^{centrifugal\ force} + \overbrace{\dot{\boldsymbol{n}}\times\boldsymbol{\rho}}^{=0} \\ &= \ddot{\boldsymbol{\rho}}|_{syn} + 2n\Big(-\dot{\eta},\dot{\xi},0\Big) - n^2(\xi,\eta,0) + 0\end{aligned} \tag{11.4.5}$$

with

$$\begin{aligned}\dot{\boldsymbol{\rho}}|_{syn} &:= \dot{\xi}\boldsymbol{u}_\xi + \dot{\eta}\boldsymbol{u}_\eta + \dot{\zeta}\boldsymbol{u}_\zeta \\ \ddot{\boldsymbol{\rho}}|_{syn} &:= \ddot{\xi}\boldsymbol{u}_\xi + \ddot{\eta}\boldsymbol{u}_\eta + \ddot{\zeta}\boldsymbol{u}_\zeta\end{aligned}$$

leading to the equations of motion in the synodic reference frame

$$\begin{pmatrix}\ddot{\xi} - 2n\dot{\eta} - n^2\xi \\ \ddot{\eta} + 2n\dot{\xi} - n^2\eta \\ \ddot{\zeta}\end{pmatrix} = -n^2\frac{\partial U'}{\partial\boldsymbol{\rho}}$$

Defining the dimensionless time and the differential operator

$$\begin{aligned}\tau &:= n\,t \\ (\,)' &:= \frac{d}{d\tau}\end{aligned}$$

yields the dimensionless form

$$\begin{aligned}&\begin{pmatrix}\xi'' - 2\eta' - \xi \\ \eta'' + 2\xi' - \eta \\ \zeta''\end{pmatrix} = -\frac{\partial U'}{\partial\boldsymbol{\rho}} \\ &= -\frac{1-\mu}{\Delta\rho_1^3}\begin{pmatrix}\xi+\mu \\ \eta \\ \zeta\end{pmatrix} - \frac{\mu}{\Delta\rho_2^3}\begin{pmatrix}\xi-(1-\mu) \\ \eta \\ \zeta\end{pmatrix}\end{aligned} \quad \textbf{EoM in the CR3BP} \tag{11.4.6}$$

where the latter follows by differentiating U' from Eqs. (11.4.4) with (11.4.3). This is the differential equation of motion (EoM) (actually three coupled scalar equations) of a small body at $\boldsymbol{\rho} = (\xi,\eta,\zeta)$ moving in the normalized gravitational potential U' (see Eq. (11.4.4)) of a minor primary with reduced mass μ at $\xi_2 = 1-\mu$ plus a major primary with reduced mass $1-\mu$ at location $\xi_1 = -\mu$ expressed in the synodic (co-rotating) barycentric reference frame.

Because the equations of motion are coupled via $\Delta\rho_i^{-3} = \Big[(\xi-\xi_i)^2 + \eta^2 + \zeta^2\Big]^{-3/2}$ they are too complex to be solved analytically. Only for specific regions, namely in the vicinity of the libration points, we are able to linearize the equations and thus derive analytical solutions. This will be done in Sects. 11.5.1 and 11.5.2. Although not being able to solve the general case analytical, we are capable to furnish general conclusions about the motion of the test mass to which we turn now.

11.4.2 Jacobi's Integral

Though we are not able to solve the above equations of motion it might be surprising to see that we can at least integrate them once. For that we first rewrite Eq. (11.4.6) in vectorial form

$$\boldsymbol{\rho}'' + 2\hat{\boldsymbol{n}} \times \boldsymbol{\rho}' - (\xi, \eta, 0) + \frac{\partial U'}{\partial \boldsymbol{\rho}} = 0$$

We then multiply this equation by the velocity vector $\boldsymbol{\rho}' = (\xi', \eta', \zeta')$. Because $(\hat{\boldsymbol{n}} \times \boldsymbol{\rho}') \cdot \boldsymbol{\rho}' = (\boldsymbol{\rho}' \times \boldsymbol{\rho}') \cdot \hat{\boldsymbol{n}}$ we get

$$\boldsymbol{\rho}' \, \boldsymbol{\rho}'' - \left(\xi\xi' + \eta\eta'\right) + \frac{\partial U'}{\partial \boldsymbol{\rho}} \boldsymbol{\rho}' = 0$$

This equation is suited to be integrated directly yielding

$$\frac{1}{2} v^2 - \frac{1}{2}\left(\xi^2 + \eta^2\right) + U' = C \quad \textbf{Jacobi's integral} \tag{11.4.7}$$

with $v^2 = \boldsymbol{v}^2 := \boldsymbol{\rho}'^2 = \xi'^2 + \eta'^2 + \zeta'^2$. C is the integration constant, which is called **Jacobi constant**. *Jacobi's integral of motion* or *Jacobi's integral* for short is a normalized conservation of energy equation for the moving test mass because it relates all energies of m normalized to dimensionless numbers: The first term on the left side corresponds to its kinetic energy, the second term to its rotational energy, and U', of course, is the normalized potential energy. Finally, the Jacobi constant C corresponds via $C = \varepsilon_{tot}/(d^2 n^2)$ to the specific total energy of m.

Conservation of energy for the test mass holds, because in the synodic system the primaries maintain fixed positions and the test mass just moves in their conservative gravitational potentials and the conservative rotational potential of the rotating synodic system. Note that in an inertial reference frame the primaries move and exchange energy with the test mass via the gravitational interaction. Therefore, the energy of the test mass is not conserved in the inertial reference frame where it constantly gains or looses energy. On this energy transfer property hinges the flyby maneuver (see Sect. 9.5).

Rotational Potential in the Synodic System

It may be confusing that in the energy conservation Eq. (11.4.7) the rotational energy and with it the rotational potential $U_\omega := E_\omega/m = -\frac{1}{2}\omega^2(x^2 + y^2) = -\frac{1}{2}\omega^2 r^2$ is negative, exactly opposite to what we would expect (see Eq. (7.2.16)).

The reason is the following. The centrifugal force of course always points outward, i.e., $\boldsymbol{F}_\omega = m\omega^2\boldsymbol{r}$. According to Eq. (7.1.5) the corresponding rotational potential is determined by

$$U_\omega = -\frac{1}{m}\int \boldsymbol{F}_\omega \cdot d\boldsymbol{r} = -\int \omega^2 r \cdot dr$$

In an inertial (sidereal) reference frame $h = \omega \cdot r^2$ (see Eq. (7.2.7)) is constant and therefore

$$U_\omega = -\int \omega^2 r \cdot dr = -h^2 \int \frac{dr}{r^3} = \frac{1}{2}\frac{h^2}{r^2} = \frac{1}{2}\omega^2 r^2 \quad @ \text{ inertial reference frame}$$

However, in a co-rotating synodic reference frame $\omega = const$ and therefore

$$U_\omega = -\omega^2 \int r \cdot dr = -\frac{1}{2}\omega^2 r^2 \quad @ \text{ synodic reference frame}$$

So, while in the inertial system the rotational energy $E_\omega = m \cdot U_{rot} = 1/2\, mh^2/r^2$ is positive, it is negative in the synodic system: $E_\omega = -1/2\, m\omega^2 r^2$ (see Fig. 11.10).

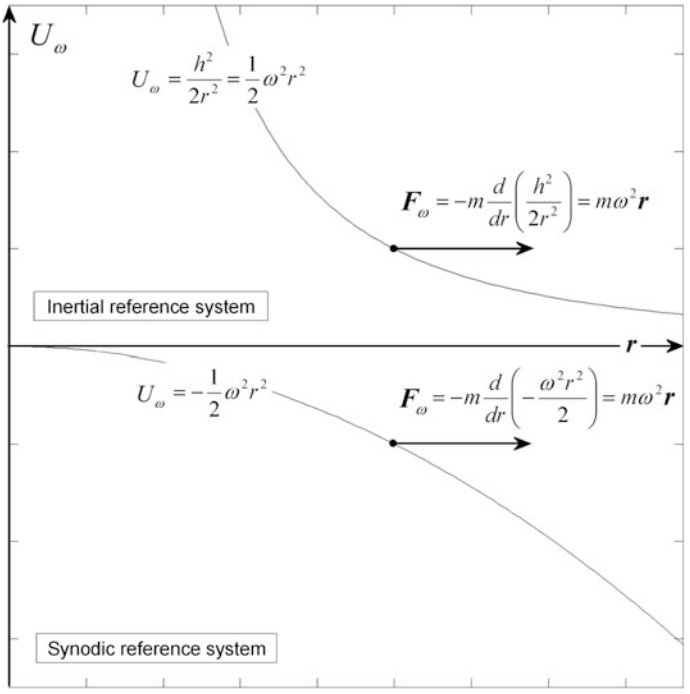

Fig. 11.10 Centrifugal potential and centrifugal force in an inertial and a synodic system

In both cases the energy decreases with increasing distance from the origin, in a way that the gradient always forms the same centrifugal force. Because the rotational potential (energy) is negative in the synodic system, one speaks of a potential field—comparable to a gravitational field, which is negative as well—which creates a fictitious force (centrifugal force). Here "fictitious" does not mean that the force is not real, but a real force that fictitiously acts from the outside. In rotating reference frames fictitious forces occur as centrifugal or Coriolis forces (the latter if a body is moving in this frame). In an inertial reference frame both types can be understood to be caused by inertial forces.

Effective Potential

In view of Eq. (11.4.7) and taking Eq. (11.4.4) into account we define for future convenience and in line with literature the *positive* effective potential

$$\Omega := \frac{1}{2}\left(\xi^2 + \eta^2\right) + \frac{1-\mu}{\Delta\rho_1} + \frac{\mu}{\Delta\rho_2} > 0 \quad \textbf{effective potential} \tag{11.4.8}$$

Its important shape is depictured in Fig. 11.11 together with the location of the libration points.

Remark W*ith a positively defined potential we dissent from physical conventions, see Eq.* (7.1.3)*, which defines potentials U negatively. We hence use with* Ω *a greek symbol rather than U. In literature the positively defined effective potential (a.k.a. "pseudopotential" due to the fictitious centrifugal force) is frequently denoted as U, too.*

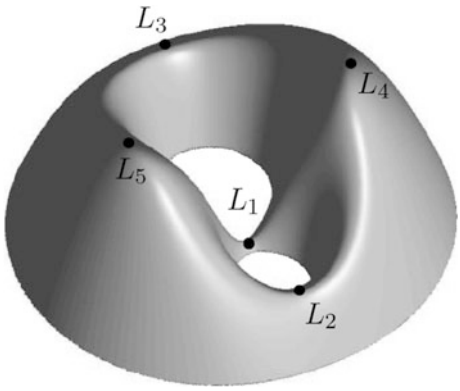

Fig. 11.11 Effective potential Ω and libration points in the CR3BP. MATLAB plot

With the effective potential we can rewrite Jacobi's integral in the form

$$\frac{1}{2}v^2 - \Omega = C \quad \textbf{Jacobi's integral} \tag{11.4.9}$$

For bounded orbits, as considered in the following, the total energy ε_{tot} and with it also C are negative, $C<0$, otherwise for an unbounded motion $C \geq 0$. Its actual value is determined from the initial conditions. It can be shown (see Problem 11.6) that for a stationary test mass at the libration points and for $m \to 0$ the Jacobi constant is given as $C_{L1} = C_{L2} = C_{L3} = -3/2$.

Note *In literature the Jacobi constant for bounded orbits often is positively defined, i.e.,* $C := \Omega - \frac{1}{2}v^2 > 0$*, or even* $C := 2\Omega - v^2 > 0$.

Because $\partial\Omega/\partial\boldsymbol{\rho} = -(\xi, \eta, 0) + \partial U'/\partial\boldsymbol{\rho}$ we can rewrite the EoM (11.4.6) as

$$\begin{aligned}\begin{pmatrix} \xi'' - 2\eta' \\ \eta'' + 2\xi' \\ \zeta'' \end{pmatrix} &= \frac{\partial\Omega}{\partial\boldsymbol{\rho}} \\ = \begin{pmatrix} \xi \\ \eta \\ 0 \end{pmatrix} &- \frac{1-\mu}{\Delta\rho_1^3}\begin{pmatrix} \xi+\mu \\ \eta \\ \zeta \end{pmatrix} - \frac{\mu}{\Delta\rho_2^3}\begin{pmatrix} \xi-(1-\mu) \\ \eta \\ \zeta \end{pmatrix}\end{aligned} \tag{11.4.10}$$

Remark *The positions of the libration points in the CR3BP of course may also be derived from the static equilibrium conditions* $\boldsymbol{\rho}'_L = \boldsymbol{\rho}''_L = 0$ *and thus according to the above equation from* $(\partial\Omega/\partial\boldsymbol{\rho})_L = 0$*. In Sects. 11.3.1 and 11.3.2 we rather adopted the derivation from the motion in the inertial system, because then it becomes clear that the libration points are just special cases of the general collinear and equilateral configurations and therefore also bear their characteristics.*

11.4.3 Stability at Libration Points

From Sect. 11.2 we already know that collinear and equilateral libration points quite generally are not stable, and hence in particular not in the CR3BP. From Fig. 11.11 we can see why and even in which way. Because the test body m always tends to decrease its potential energy (and in return gains speed) it will "move down the hills". The corresponding acceleration forces are depicted in Fig. 11.12. For the two equilateral points the situation is clear: Any direction is downhill (blue arrows). Therefore these points must be statically unstable.

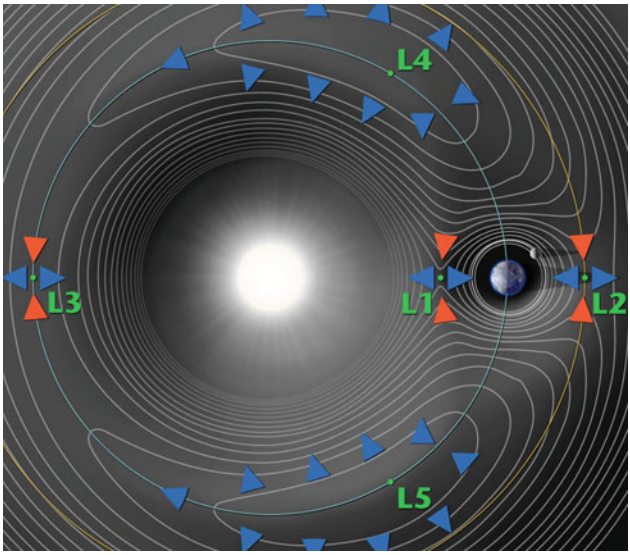

Fig. 11.12 Equipotential lines of the effective potential Ω and the stabilizing (red) and destabilizing forces (blue) at the libration points in the Sun-Earth system resulting from it. *Credit* NASA

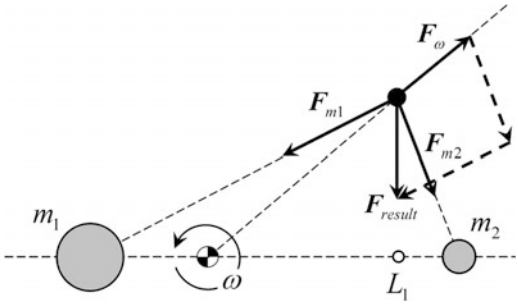

Fig. 11.13 The restoring force (resultant arrow F_{result}) of a body near L_1 resulting from the gravitational forces (thick arrows F_{m1} and F_{m2}) and the centrifugal force (thick arrow F_ω)

For the collinear points the destabilizing forces (blue arrows in Fig. 11.12) point along the direction of the configuration line. Therefore they are unstable. However, perpendicular to this line there are restoring forces (red arrows, both in the Moon's motion plane and vertically to it, not shown here) that push the mass m back to the collinear points. This restoring effect is comprehensible, as the resultant from the gravitational forces and the centrifugal force points in the direction of L_1 (see Fig. 11.13). So the shapes of the potential at the three collinear points are saddles (see Fig. 11.11).

In Sect. 11.5.2 it will be shown that if you bring a spacecraft to a collinear libration point L_1 or L_2 and leave it to its own without any station-keeping measures, small initial deviations Δx_0 along the configuration line would exponentially increase according to

$$\Delta x = \Delta x_0 \cdot \exp(t/\tau) \tag{11.4.11}$$

The e-folding relaxation time τ can be derived from Eq. (11.5.8) with $c_2 = 4$ (see Eq. (11.5.6)) to be

$$\tau = \frac{T}{2\pi\sqrt{1+2\sqrt{7}}} = 0.06345 \cdot T \quad @\ L_1, L_2 \tag{11.4.12}$$

where T is the orbital period of the primary bodies. So, in the Earth–Moon system, a deviation e-folds successively every $\tau = 1.73$ days and in the Sun–Earth system $\tau = 23.2$ days.

The collinear libration point L_3 turns out to be more stable. Applying Eq. (11.5.8) with $c_2 = 1 + \frac{7}{8}\mu$ (see Eq. (11.5.6)), we obtain

$$\tau = \frac{T}{\pi}\sqrt{\frac{2(m_1+m_2)}{21m_2}} \quad @\ L_3 \tag{11.4.13}$$

For the system Earth–Moon this results in $\tau = 24.4$ days. So, compared to any other fixed position in the Earth–Moon system, considerably less station-keeping effort along the configuration line and hence less propellant is required.

11.4.4 General System Dynamics

In Sect. 11.1.1 we already mentioned that for the general n-body problem (n bodies with arbitrary mass and with arbitrary initial conditions) there exist no algebraic integrals of motion other than the classical conservation laws. In this general case we would not have any information on the motion of the test body. The only possibility would be to solve the equations of motion numerically. In the special case of the CR3BP we have found with Jacobi's integral Eq. (11.4.9) an additional conditional equation that restricts the motion of the test body and thus provides some general information about its motion.

To figure out what this additional integral brings about we recall the motion of a body in a central effective potential U_{eff} in the two-body problem as given by Eq. (7.2.19) and depicted in Fig. 7.7. There we saw that the specific total energy restricts the orbital motion and thus defines a class of orbits having the same characteristics, namely elliptic, parabolic, and hyperbolic orbits. By relating the specific total energy to Jacobi's integral we now want to convey this property to the motion of a body in the effective potential Ω the CR3BP.

We therefore define the class of all trajectories having a given Jacobi constant C, i.e., a given total energy, as **invariant manifolds**. Manifolds of dynamical systems can be pictured quite generally as 2D topological subspaces in our common 3D space. A specific manifold represents the phase space of a system's dynamics. Owing to the property of constant total energy, invariant manifolds have the

additional property that a body's trajectory in this phase space that starts out in an invariant manifold remains in this manifold for the duration of its dynamical evolution. Mathematically speaking, the body's state flows in the manifold and therefore the manifold is said to be invariant under this flow.

The objective of this section is to study the invariant manifolds of a CR3BP in general in and Sect. 11.5 those about libration points. Generally, there are two types of invariant manifolds, namely *center manifolds*, which are the phase space of periodic and quasi-periodic orbits, and two variants of *hyperbolic manifolds, a.k.a. saddle manifolds*, namely *stable manifolds* and *unstable manifolds,* which are the phase space of orbits, which wind on or off periodic and quasi-periodic orbits, respectively, as will be discussed in Sect. 11.5.2.

Remark *Much of the nomenclature used here, such as "invariant manifold" or "flow", stems from dynamical systems theory, which deals with the behavior of non-linear systems as described by non-linear ordinary differential equations. An excellent introduction and account of dynamical system theory is given by Ledermann (1990).*

Zero-velocity Curves

We now use Jacobi's integral to determine the space that is accessible to the test mass. It ends where its velocity becomes zero. So, if we set $v = 0$ in Eq. (11.4.9), we get a curve that envelopes the space in which the body can possibly move. The test body cannot cross the envelope curve, it can touch it with velocity $v = 0$ at selected points. For a given C of the test body, the envelope curve is the line, the coordinates of which satisfy the equation $\Omega(\xi, \eta, \zeta) = -C$ and is apparently the contour line of the effective potential in Fig. 11.11. The envelope curve is also called *zero-velocity curve*, a.k.a. *Hill curve* after the astronomer Hill, who studied it in detail in the 19th century.

Let us examine in detail the zero-velocity curve and how it depends on the energy of the test mass. For a given negative C (total energy) and because kinetic energy is positive, the body can move only in those spatial areas where $-\Omega \leq C$. According to Eq. (11.4.8), this is the case whenever $\Delta\rho_1$ or $\Delta\rho_2$ is very small, i.e., when m is close to one of the bodies m_1 or m_2 (large negative gravitational energy), or when m is far a way from both (large negative rotational energy). These areas are indicated in white in Fig. 11.14 for the Earth m_1 and the Moon m_2. The inaccessible area $-\Omega > C$ in between is indicated in gray. If the energy of the test body and hence C gradually increases, the test body is able to access more and more space (Fig. 11.14). In Fig. 11.14b for $C = -1.6735$ a transit from Earth to the Moon via L_1 is possible for the first time. It shows that the flight to Moon via L_1 is energetically most favorable. If the energy of the test body is further increased, L_2 and L_3 also become accessible (Fig. 11.14c, d). The equilateral libration points L_4 and L_5 are potentially the highest points in Earth–Moon system, and are achieved in the end for $C = -1.5600$ (Fig. 11.14e, f).

The zero-velocity curves merely define the limits of motion of the test body. They do not tell us anything about how the test body moves within the permissible

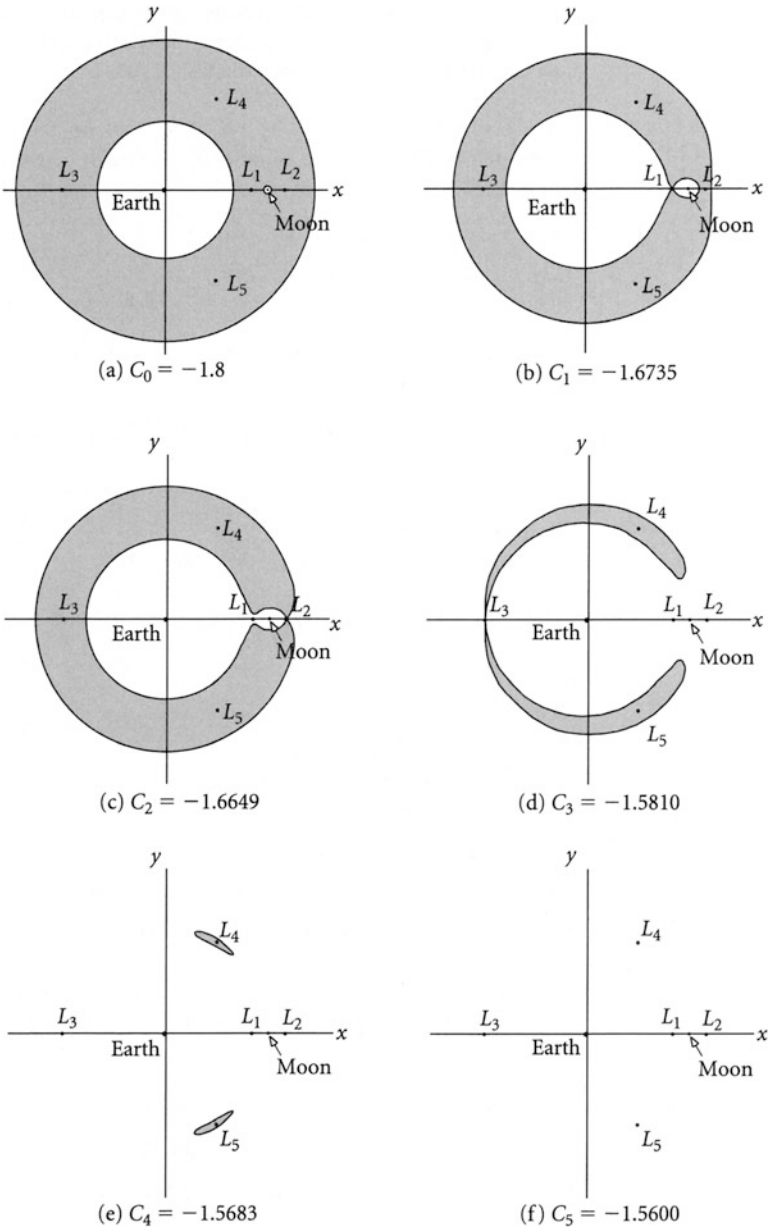

Fig. 11.14 Zero-velocity curves in the Earth–Moon system with increasing Jacobi constant C (total energy). *Credit* Curtis (2005)

areas, that is, about the distinct properties of the invariant manifolds. For instance, we know that the most favorable trajectory from Earth to Moon is via L_1, but we do not know what a corresponding trajectory looks like. To find out we have to solve the equations of motion with the initial conditions defining the energy of the test body. This will be done in the next three sections (see Fig. 11.27 for a particular Earth–Moon trajectory via L_1).

Chaotic Trajectories

Apart from the conservation of Jacobi's integral, which accounts for the zero-velocity curves, there are no limits on the trajectory of a body. So, to determine a trajectory from a given initial state vector, Eq. (11.4.10) must be solved numerically. A typical result shown in Fig. 11.15 for the Earth–Moon system. From the intricate shape of the trajectory we conclude that any tiny change in the initial state will cause increasing deviations from the original trajectory that will end up in a totally different path. Such a behaviour, being highly sensitive to the initial condition, is typical for a so-called *deterministic chaos*. It is chaotic because it is nondeterministic in the long run but deterministic in the short. Deterministic chaotic behavior is very common for motion governed by non-linear differential equations, such as the equation of motion (11.4.10). The science of deterministic chaos, the so-called *chaos theory*, is a special but important branch of *dynamical systems theory*. We do not want to go into details of chaos theory, but only mention two main characteristics.

The sensivity of the long term evolution of the system manifests itself as an exponential growth of perturbations in the initial conditions. This is explicitely demonstrated by the equation $\Delta x = \Delta x_0 \cdot \exp(t/\tau)$ of Sect. 11.4.3, which determines the stability at the libration points. The relaxation time τ is nothing else than the inverse of the so-called Lyapunov exponent in chaos theory.

Although deterministic chaotic systems are inherently unpredictable, they are easily controlable. *Control theory* deals with influencing the behavior of dynamical systems. Basic methods of controlling a chaotic orbit are the *OGY* (Ott, Grebogi and

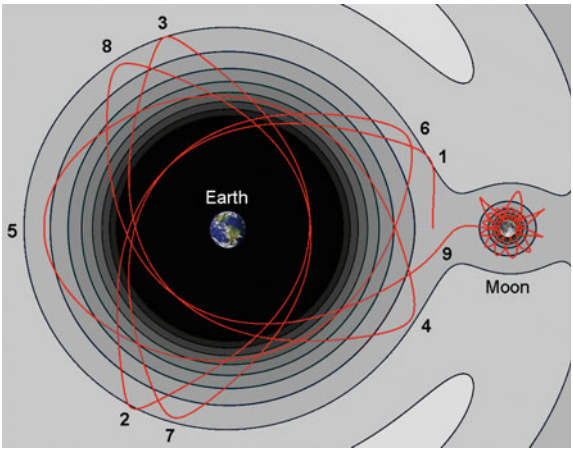

Fig. 11.15 A chaotic trajectory in the Earth–Moon system with a final moon capture. *Credit* Andreas Sandberg, Creative Commons, and U. Walter

Yorke) *method*, and *Pyragas continuous control method*. In the OGY method swift and tiny kick-burns once per cycle are applied to keep a spacecraft on a periodic target trajectory. Such kick-burns would keep for instance the spacecraft infinitely at a libration point, or adjust the trajectory in Fig. 11.15 such that the turning points $6 \rightarrow 1, 7 \rightarrow 2, 8 \rightarrow 3$, and $9 \rightarrow 4$ would coincide, leading to a closed periodic orbit. The same can be achieved by the Pyragas method, employing continuous thrust. As long as the system evolves close to the desired periodic orbit, the orbit-keeping thrust is very small, but increases rapidly when it drifts away from the target orbit.

Rapprochement Orbits

Such a closed periodic orbit belongs to the numerous class of highly symmetrical periodic orbits. Among those there is a special class of highly symmetrical periodic orbits with the additional feature that the body approaches one or both primaries repeatedly and very closely. This is why this type of orbit is called a rapprochement orbit. French mathematicians extensively studied these orbits, in particular for the Earth–Moon case.

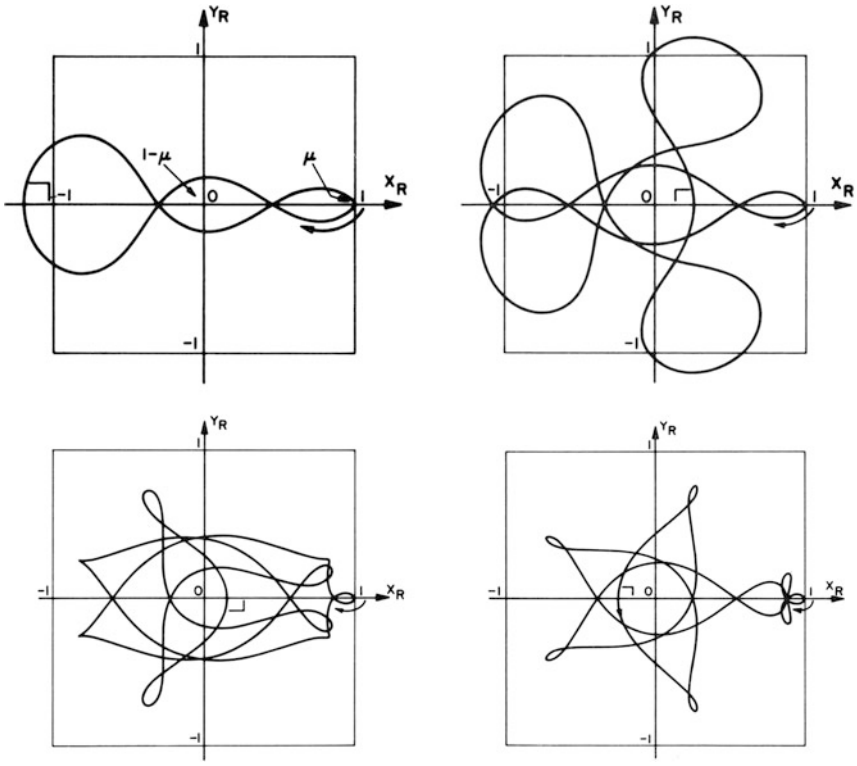

Fig. 11.16 Four typical rapprochement orbits in the Earth–Moon system. *Credit* Hoelker R.F., NASA TN D-5529

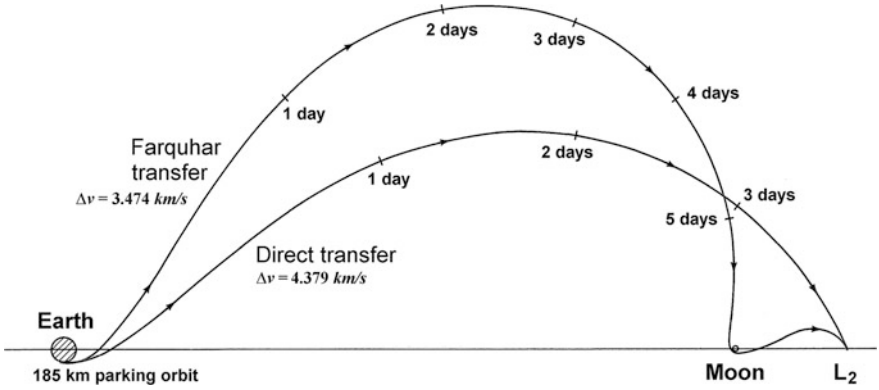

Fig. 11.17 A three-impulse Farquhar transfer orbit based on a rapprochment orbit from a 185 km Earth parking orbit to the LL_2 point (with stopping) with $\Delta v = 3.474\,km/s$ taking 212 hours compared to a two-impulse direct transfer with $\Delta v = 4.379\,km/s$ taking 96 hours. (*Credit* Farquhar, R. W. / NASA-GSFC (1971))

Figure 11.16 shows four typical rapprochement orbits. The transfer body infinitely shuttles on a symmetrically closed curve between Earth and Moon. The practical application of rapprochement orbits is their use to commute to a primary or between the primaries. There is an immense number of rapprochement orbits, which, however, share the property of all chaotic systems: Any tiny initial perturbation, if uncorrected, amplifies until the orbit is no longer symmetrical–periodical, but takes on a chaotic course. However, as we have learned above, keeping a rapprochement orbit in symmetrical shape requires little effort.

There are variants of these orbits that are interesting from another practical point of view, e.g., low energetic transfer orbits to the libration points between Earth and Moon. Figure 11.17 shows such a low energy orbit to libration point L_2, which was studied by Farquhar and coworkers and which is anticipated to be utilized for the SLS Exploration Mission One (EM-1) in 2020. It takes advantage of a special flyby past the Moon to swing by to L_2.

Free-Return Trajectories

When mission planning for the first manned US missions to the Moon was at issue, the safety of the crew in case of a main engine failure played a crucial role. Thus a trajectory was selected that assured the return of the astronauts to the Earth even with a total main engine failure. This special circumlunar trajectory was called "free-return" trajectory and it is depicted in Fig. 11.18. It is a symmetrical-periodical trajectory, and thus is a rapprochement orbit. It passes the surface of the Moon with a minimum distance of 111 km, which corresponds exactly to the

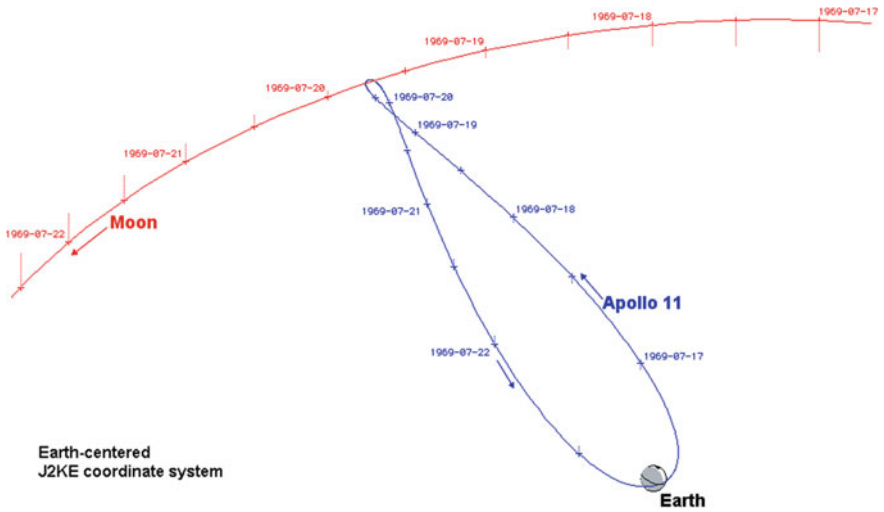

Fig. 11.18 The reconstructed circumlunar, free-return trajectory of Apollo 11 to the Moon. *Credit* Simulation by Daniel R. Adamo

periselene altitude of the missions Apollo 8, 10, and 11. Later Moon-landing missions entered into a circular Moon orbit at this point, from which it was then possible to descent to the Moon's surface. If the mission had to be aborted for any reason, the engine ignition required for braking behind the Moon into the circular Moon orbit would not have happened, and the astronauts would automatically have returned to the Earth. This indeed happened with Apollo 13.

The trajectory shown in Fig. 11.18 is fully symmetric with regard to the Earth–Moon connecting line. The actual trajectories of the Apollo missions were slightly asymmetric, such that on return the spacecraft would touch the Earth's atmosphere in order to guarantee an automatic reentry. This asymmetry was achieved by a slight shift of the position of the periselene.

During the outward as well as return flight the free-return trajectory is clearly elliptical in the proximity of the Earth, as the gravitational influence of the Earth is dominating. Approaching the edge of the Moon's SOI (see Sect. 9.1) the trajectory becomes more and more a straight line: here the orbital velocity has already decreased quite a lot, and the gravitational influence of the Earth and the Moon plus centrifugal force just cancel out each other. In this area the real trajectory deviates utmost from the patched-conics approximation. In the surroundings of the Moon the trajectory is bent into a hyperbola.

11.5 Dynamics About Libration Points

11.5.1 Equation of Motion

In the following we want to explore the trajectories in the vicinity of the five libration points L, the location of which we denote in the barycenter system (see Fig. 11.9) by

$$\boldsymbol{\rho}_L = (\xi_L, \eta_L, 0)$$

From the results of Sects. 11.3.1 and 11.3.2, and because $\xi_L = \Delta x/d + \xi_1 = \Delta x/d - \mu$ we have the results in Table 11.2. In order to derive the equations of motion about libration points we define the position vector $\boldsymbol{r} = (x, y, z)$ relative to a libration point under consideration (see Fig. 11.9)

$$\boldsymbol{\rho} =: \boldsymbol{\rho}_L + \boldsymbol{r} \tag{11.5.1}$$

Note that we reuse the notation $\boldsymbol{r}$ (cf. Eq. (11.4.1)) for convenience and because it is also used quite often in literature. For the position of the primaries relative to this libration point

$$\boldsymbol{r}_i = (x_i,\, y_i,\, 0) = (\xi_i - \xi_L,\, \eta_i - \eta_L,\, 0) \quad @\ i = 1, 2 \tag{11.5.2}$$

we have with $\xi_1 = -\mu$, $\xi_2 = 1 - \mu$, and ξ_L, μ_L from Table 11.2 the results listed also in Table 11.2.

Because from Eq. (11.5.1) $0 = \eta_i = \eta_L + y_i$ and hence $\eta = \eta_L + y = y - y_i$, we have $\Delta\rho_i = \sqrt{(\xi - \xi_i)^2 + \eta^2 + \zeta^2} = \sqrt{(x - x_i)^2 + (y - y_i)^2 + z^2}$. This gives rise to the definition

$$\Delta r_i := \sqrt{(x - x_i)^2 + (y - y_i)^2 + z^2} \tag{11.5.3}$$

Table 11.2 Positions ξ_L, μ_L of the libration points in the barycentric synodic reference frame and positions x_1, y_1 and x_2, y_2 of the two primaries relative to the libration points

	L_1	L_2	L_3	L_4	L_5
ξ_L	$\Delta_1 - \mu$	$\Delta_2 - \mu$	$-\Delta_3 - \mu$	$0.5 - \mu$	$0.5 - \mu$
η_L	0	0	0	$+\sqrt{3}/2$	$-\sqrt{3}/2$
x_1	$-\Delta_1$	$-\Delta_2$	Δ_3	–0.5	–0.5
y_1	0	0	0	$-\sqrt{3}/2$	$+\sqrt{3}/2$
x_2	$1 - \Delta_1$	$-(\Delta_2 - 1)$	$1 + \Delta_3$	+0.5	+0.5
y_2	0	0	0	$-\sqrt{3}/2$	$+\sqrt{3}/2$

and therefore

$$\frac{\partial\Omega}{\partial\boldsymbol{\rho}} = \frac{\partial\Omega}{\partial\boldsymbol{r}} = \begin{pmatrix} x \\ y \\ 0 \end{pmatrix} + \boldsymbol{\rho}_L + \frac{\partial}{\partial\boldsymbol{r}}\left(\frac{1-\mu}{\Delta r_1} + \frac{\mu}{\Delta r_2}\right)$$

Inserting these results into our master Eq. (11.4.10) we obtain

$$\begin{aligned} &\begin{pmatrix} x'' - 2y' - x \\ y'' + 2x' - y \\ z'' \end{pmatrix} = \frac{\partial\Omega}{\partial\boldsymbol{r}} - \begin{pmatrix} x \\ y \\ 0 \end{pmatrix} \\ &= \boldsymbol{\rho}_L + \frac{\partial}{\partial\boldsymbol{r}}\left(\frac{1-\mu}{\Delta r_1} + \frac{\mu}{\Delta r_2}\right) \\ &= \boldsymbol{\rho}_L - \left[\frac{1-\mu}{\Delta r_1^3}\begin{pmatrix} x - x_1 \\ y - y_1 \\ z \end{pmatrix} + \frac{\mu}{\Delta r_2^3}\begin{pmatrix} x - x_2 \\ y - y_2 \\ z \end{pmatrix}\right] \end{aligned} \qquad \textbf{EoM about a libration point} \qquad (11.5.4)$$

These are the equations of motion of a small moving body at the normalized distance $\boldsymbol{r} = (x, y, z)$ from any of the five libration points, with Δr_1, Δr_2 given by Eq. (11.5.3) and x_1, y_1, x_2, y_2 given by Table 11.2 expressed in the synodic (co-rotating) barycentric reference frame.

In the following we will study the dynamics in the vicinity of libration points (For more details the book Perozzi (2010) is recommended). To do so we have to distinguish between collinear and equilateral libration points.

11.5.2 Collinear Libration Points

We first consider the detailed dynamics in the vicinity the collinear libration points L_1, L_2, L_3.

Equation of Motion

In the vicinity of a collinear libration point $\boldsymbol{r} \approx 0$ and therefore we are able to evaluate the upper right side of Eq. (11.5.4) in powers of r. To do so, and because for any collinear libration point $y_i = 0$ holds, we first write

$$\begin{aligned} \Delta r_i &= \sqrt{(x - x_i)^2 + y^2 + z^2} = |x_i|\sqrt{\left(\frac{x}{x_i} - 1\right)^2 + \left(\frac{y}{x_i}\right)^2 + \left(\frac{z}{x_i}\right)^2} \\ &= |x_i|\sqrt{1 - 2\frac{x}{r}\frac{r}{x_i} + \left(\frac{r}{x_i}\right)^2} \end{aligned}$$

Now, according to mathematical tables, $1/\sqrt{1-2\alpha u+u^2}$ is the generating function of the Legendre polynomials P_n of degree n

$$\frac{1}{\sqrt{1-2\alpha u+u^2}}=\sum_{n=0}^{\infty}u^n P_n(\alpha)$$

Identifying $\alpha\equiv x/r$ and $u\equiv r/x_i$ we therefore find for the power series in r

$$\frac{1}{\Delta r_i}=\frac{1}{|x_i|}\sum_{n=1}^{\infty}\left(\frac{r}{x_i}\right)^n P_n\left(\frac{x}{r}\right)$$

Inserting this and x_i from Table 11.2 into Eq. (11.5.4) we find for the equation of motion

$$\begin{pmatrix}x''-2y'-x\\ y''+2x'-y\\ z''\end{pmatrix}=\boldsymbol{\rho}_L+\frac{\partial}{\partial\boldsymbol{r}}\left(\frac{1-\mu}{\Delta r_1}+\frac{\mu}{\Delta r_2}\right)=\boldsymbol{\rho}_L+\frac{\partial}{\partial\boldsymbol{r}}\sum_{n=1}^{\infty}c_n r^n P_n\left(\frac{x}{r}\right)\quad(11.5.5)$$

with

$$c_n=\operatorname{sgn}(x_1)\frac{1-\mu}{x_1^{n+1}}+\operatorname{sgn}(x_2)\frac{\mu}{x_2^{n+1}}$$

For $n=0$ we have $\partial/\partial\boldsymbol{r}(c_0P_0)=\partial/\partial\boldsymbol{r}(c_0\cdot 1)=0$. Evaluating the term for $n=1$ we have with $P_1(\alpha)=\alpha$ and Eqs. (11.4.3), (11.4.4), (11.4.5) and Table 11.2 $c_1=-\xi_L$ and hence

$$\frac{\partial}{\partial\boldsymbol{r}}\left[c_1 r P_1\left(\frac{x}{r}\right)\right]=\frac{\partial}{\partial\boldsymbol{r}}(c_1x)=\begin{pmatrix}c_1\\0\\0\end{pmatrix}=-\boldsymbol{\rho}_L$$

With this and applying for $n=2$ the same procedure to $P_2(\alpha)=\frac{1}{2}(3\alpha^2-1)$ we can rewrite the EoM (11.5.4) as

$$\begin{pmatrix}x''-2y'-(1+2c_2)x\\ y''+2x'\quad-(1-c_2)y\\ z''\qquad\qquad+c_2z\end{pmatrix}=\frac{\partial}{\partial\boldsymbol{r}}\sum_{n=3}^{\infty}c_n r^n P_n\left(\frac{x}{r}\right)\qquad\textbf{EoM near } \boldsymbol{L_1, L_2, L_3}\quad(11.5.6)$$

with

$$c_2=\begin{cases}\frac{1-\mu}{\Delta_1^3}+\frac{\mu}{(1-\Delta_1)^3}=4+6\lambda+O(\lambda^2) & @\ L_1\\ \frac{1-\mu}{\Delta_2^3}+\frac{\mu}{(\Delta_2-1)^3}=4-6\lambda+O(\lambda^2) & @\ L_2\\ \frac{1-\mu}{\Delta_3^3}+\frac{\mu}{(1+\Delta_3)^3}=1+\frac{7}{8}\mu+O(\mu^2) & @\ L_3\end{cases},$$

and

$$\lambda=\left(\frac{\mu}{3}\right)^{1/3},\quad \mu=\frac{m_2}{m_1+m_2}$$

where the latter follows from employing the power series expansions of Eq. (11.3.7). These are the equations of motion of a small moving body at $\boldsymbol{r} = (x, y, z)$ (dimensionless) in the vicinity of and relative to a collinear libration point in the synodic reference frame.

Invariant Manifolds

In celestial mechanics the investigation of these coupled equations of motion and the study of their general behavior is currently an ongoing research in order to design for instance space telescope missions to L_1 or L_2 points in the Sun–Earth and Earth–Moon systems. The differential Eqs. (11.5.6) are quite complex and can generally be solved only numerically. However, without knowing the detailed solution we can study the types of solutions and their fundamental behavior. This fundamental behavior is already captured by the linear part, which is the left sides of Eq. (11.5.6). The right sides are in the vicinity of the collinear libration points minor, non-linear modifications. We therefore study in the following the linearized equations

$$\boxed{\begin{array}{lll} x'' - 2y' - (1+2c_2)x = 0 \\ y'' + 2x' \;\; - (1-c_2)y = 0 \\ z'' \qquad\qquad + c_2 z = 0 \end{array}} \quad \textbf{linearized EoM} \tag{11.5.7}$$

Upon solving these linearized differential equations one notices that the third equation is decoupled from the other two and displays the behavior of a harmonic oscillator with frequency $\omega_z = \sqrt{c_2}$. For the other two equations we make the standard ansatz for linear differential equations, $x = x_0 \exp(\lambda\tau)$, $y = y_0 \exp(\lambda\tau)$, and find for the characteristic polynomial

$$\lambda^4 + (2 - c_2)\lambda^2 + (1 + 2c_2)(1 - c_2) = 0$$

of the matrix

$$\boldsymbol{A} = \begin{pmatrix} 0 & 0 & 1 & 0 \\ 0 & 0 & 0 & 1 \\ 1+2c_2 & 0 & 0 & 2 \\ 0 & 1-c_2 & -2 & 0 \end{pmatrix}$$

which satisfies $\boldsymbol{X}' = \boldsymbol{A}\boldsymbol{X}$, where $\boldsymbol{X} = (x, y, x', y')$. Considered as a quadratic characteristic equation for λ^2 we find that, because of $c_2 > 1$ (see Eq. (11.5.6)) the sign changes only once between consecutive terms, which implies from Descartes' rule of signs that λ^2 has a positive and a negative root, namely

$$\lambda_-^2 = \frac{1}{2}\left(c_2 - 2 - \sqrt{9c_2^2 - 8c_2}\right) < 0$$
$$\lambda_+^2 = \frac{1}{2}\left(c_2 - 2 + \sqrt{9c_2^2 - 8c_2}\right) > 0$$

By assigning the solutions $\lambda_{xy} = \pm i\sqrt{-\lambda_-^2} =: \pm i\omega_{xy}$ and $s = \pm\sqrt{\lambda_+^2}$ we find that the solutions of the linearized EoM (11.5.7) quite generally can be written as

$$\begin{aligned} x &= A_1 e^{s\tau} + A_2 e^{-s\tau} + A_x \cos\left(\omega_{xy}\tau + \phi\right) \\ y &= a(A_1 e^{s\tau} - A_2 e^{-s\tau}) + bA_x \sin\left(\omega_{xy}\tau + \phi\right) \\ z &= A_z \cos(\omega_z \tau + \psi) \end{aligned} \tag{11.5.8}$$

where

$$a = \frac{s^2 - 1 - 2c_2}{2s}, \quad b = -\frac{1 + 2c_2 + \omega_{xy}^2}{2\omega_{xy}}$$

Note that owing to the normalization of the EoM the angular frequencies ω_{xy}, ω_z are actually in units $n = \sqrt{G(m_1 + m_2)/d^3} = 2\pi/T$, i.e., the orbital frequency of the synodic system. To give an example: In the Sun–Earth synodic system we have at L_1 and L_2

	c_2	ω_{xy}	ω_z	s	a	b
L_1	4.061012	2.07184	2.00025	2.50869	−0.53982	−3.20839
L_2	3.940522	2.05701	1.98507	2.48432	−0.54526	−3.18723

The coefficients A_1, A_2, A_{xy}, A_z and phase angles ϕ, ψ are determined from the initial conditions $x_0, y_0, z_0, x_0', y_0', z_0'$. So, the initial conditions that determine the Jacoby constant C, plus Eq. (11.5.8) are the clue to finding the C-invariant manifolds, i.e., the classes of trajectories.

Before we now turn into a discussion of the trajectories we have to recall that the equations of motion Eq. (11.5.6) in fact have a non-linear right-hand side, which becomes increasingly significant as the motion departs from the collinear libration point. This non-linear part effectively modifies all the above trajectory parameters $\omega_{xy}, \omega_z, s, a, b$. Most importantly, the frequencies ω_{xy}, ω_z start to vary with larger amplitudes A_x, A_z of their orbits.

Keeping this in mind we can read off Eq. (11.5.8) the following general behavior: Depending on the initial conditions there are unbounded solutions for $A_1, A_2 \neq 0$ and stable periodic solutions for $A_1, A_2 = 0$. This is in accordance with the *center manifold theorem* stating that associated with each imaginary eigenvalue of the Jacobian matrix $\boldsymbol{A}$ there exists a bounded so-called center manifold and to each real eigenvalue and an unbounded hyperbolic manifold (saddle). So we have at

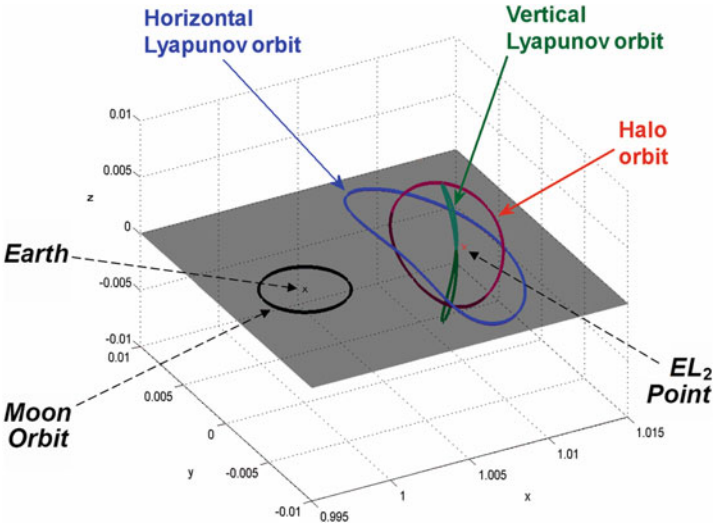

Fig. 11.19 Three of four periodic orbits about the EL_2 point in the Sun–Earth system: the two Lyapunov orbits and a southern halo orbit. *Credit* Egemen Kolemen (2012)

each equilibrium point a center × center × saddle type of solutions with accordingly bounded and unbounded orbits.

Center Manifold Orbits

When the oscillatory amplitudes are very small, i.e., when we are in the linear limit, there are two types of periodic orbits (see Fig. 11.19):

1. **Vertical Lyapunov orbits** for $A_1, A_2, A_x = 0$ and $A_z \neq 0$, which are vertical periodic motions with frequency ω_z along the z-axis, and a
2. **Horizontal Lyapunov orbits** (a.k.a. planar Lyapunov orbit) for $A_1, A_2, A_z = 0$ and $A_x \neq 0$, which are near-elliptic motions in the x–y plane with frequency ω_{xy} and with semi-major axis along the y-axis being $b \approx 3.2$ times the semi-minor axis along the x-axis.

For $A_x, A_z \neq 0$ amplitudes we find quasi-periodic 2D tori orbits, so-called **Lissajous orbits**, with motion amplitudes in all three axis revolving either Lyapunov orbit (see Fig. 11.20). Depending on the concrete initial A_x, A_z, Lissajous orbits occur in many different sizes and shapes that can even occur as crossovers between vertical and horizontal Lyapunov orbits. Lissajous orbits in general do not close and exhibit $\omega_{xy} > \omega_z$ (see above table). If we increase the energy of the orbits by increasing the amplitudes, and via the non-linear terms of the EoM thus also ω_{xy}, ω_z, there might be cases when ω_{xy}/ω_z becomes a rational value, in which case we get closed periodic Lissajous orbits.

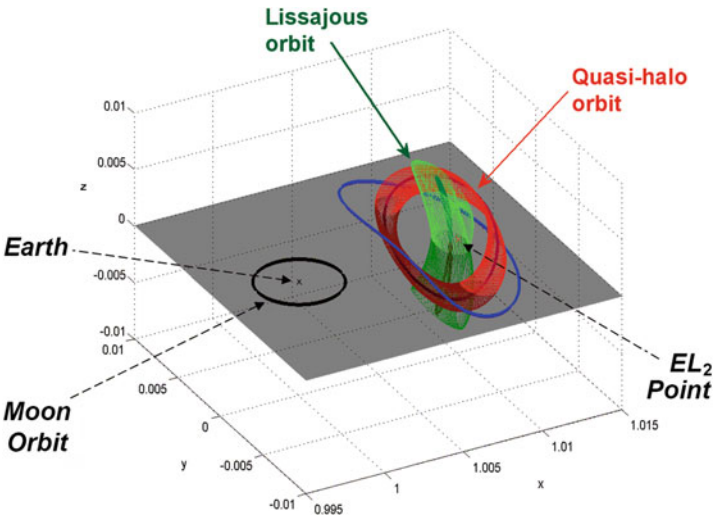

Fig. 11.20 Two quasi-periodic orbits about the EL_2 point in the Sun–Earth system: a Lissajous orbit revolving the vertical Lyapunov orbit and a southern quasi-halo orbit. *Credit* Egemen Kolemen (2012)

When the very special case $\omega_{xy} = \omega_z$ is attained (For a motion about the L_2 point in the Sun–Earth system this happens for $A_x \approx 200\,000$ km) two new periodic orbits, the so-called northern and southern **halo orbits** (for the definition of *northern* and *southern* see below) bifurcate from the horizontal Lyapunov orbit (see Fig. 11.19). For $\omega_{xy} \approx \omega_z$ we have quasi-periodic orbits around these halo orbits, so-called **quasi-halo orbits** (see Fig. 11.20). In between the Lissajous and quasi-halo orbits chaotic behavior occurs (see Fig. 11.22). Because the c_2 coefficient in the linearized EoM (11.5.6) is nearly constant for the three collinear points, the periodic orbits about the different collinear points are very similar. The sets of phase states of the above bounded periodic and quasi-periodic orbits form the so-called *center manifold* (cf. Sect. 11.4.4), which need to be categorized from the unbounded motion to which we will return below.

Note *Precise periodic halo orbits exist only in the exact circular restricted problem. In the real world the minor primary mass (e.g. Moon revolving around the Earth) has a somewhat elliptic orbit and therefore "halo orbits" are only close to true periodic halo orbits. For this reason the term "halo orbit" or "periodic orbit" in the literature (see for instance "L1 periodic orbit" in Fig. 12.24b) usually and sloppily includes any periodic and quasi-periodic orbits, or center manifold orbits in general. In particular, the "halo orbit" of the Genesis mission as depicted in Fig. 11.28 was actually a Lissajous orbit.*

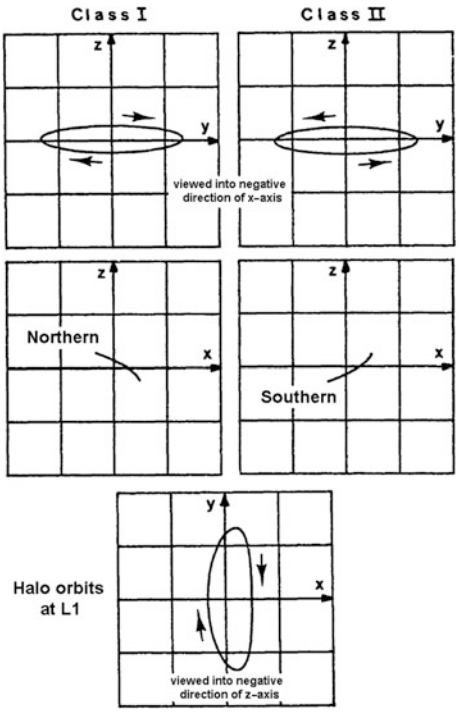

Fig. 11.21 Class I and Class II halo orbits at a L_1 point. *Credit* D. L. Richardson (1980)

Classification of Halo Orbits

According to Eq. (11.5.8) the bounded periodic or quasi-periodic motion can be written as

$$x = A_x \cos\left(\omega_{xy}\tau + \phi\right)$$
$$y = bA_x \sin\left(\omega_{xy}\tau + \phi\right)$$
$$z = A_z \cos(\omega_z\tau + \psi)$$

The periodicity of the halo orbits with $\omega_{xy} = \omega_z$ implies that the phase angles ϕ, ψ obey the relation

$$\psi = \phi + k\frac{\pi}{2}, \quad k = \pm 1$$

From this relation two types of halo orbits result:

Class I halo orbit: If $k = +1$ the sense of revolution of the body about the libration point is clockwise as viewed into the negative direction of the x-axis.

Class II halo orbit: If $k = -1$ the sense of revolution is counterclockwise as viewed into the negative direction of the x-axis.

Class I / Class II halo orbits have the property that they can be viewed as mirror images across the x–y plane as seen in the x–z plane where Class I / Class II halos have their upper turning point (in z-direction) lying on the more negative/positive side of the x-axis (see Fig. 11.21).

However, they are asymmetric about the other two planes. The reason being that the effective potential around a collinear point deviates slightly from a paraboloid, obviously being shallower and hence the halo orbit more elongated outbound from the closest primary. For instance, in the middle part of Fig. 11.23 the halo orbit is more elongated inbound to the Sun. Of course, a body on a halo orbit spends more than half of its period on the more elongated part of the orbit. This gives rise to another classification of halo orbits called

Northern/Southern halo orbit
A body on a Northern/Southern halo orbit spends more than half of its period above/below the x–y plane (in z-direction), i.e., North/South of it.

Whether a Class I or Class II halo is a Northern or Southern halo depends on whether the halo orbit is elongated inbound or outbound. Table 11.3 summarizes this mapping between the two halo classifications and gives the sense of rotation of the halo orbit as seen from the major and minor primary.

For instance, in Fig. 11.19 we have a Northern (Class II) halo orbit at L_2. This is because the upper turning point of the halo orbit lies more on the positive side of the x-axis (i.e., Class II type) and because the orbit is elongated outbound (positive x-axis) at ML_2, which is above the x–y plane (i.e., Northern type). The sense of rotation as seen from Earth (major primary) is clockwise. On the other hand we have in Fig. 11.23 for the SOHO probe at the EL_1 point a Southern (Class II) halo

Table 11.3 Relation of class-type and Northern/Southern-type at the three collinear points and sense of rotation (SOR) as seen from the major and minor primary

	L_1	L_2	L_3
Class I	**Northern**	**Southern**	**Northern**
SOR seen from major primary	Anti-clockwise	Anti-clockwise	Clockwise
SOR seen from minor primary	Clockwise	Anti-clockwise	Clockwise
Class II	**Southern**	**Northern**	**Southern**
SOR seen from major primary	Clockwise	Clockwise	Anti-clockwise
SOR seen from minor primary	Anti-clockwise	Clockwise	Anti-clockwise

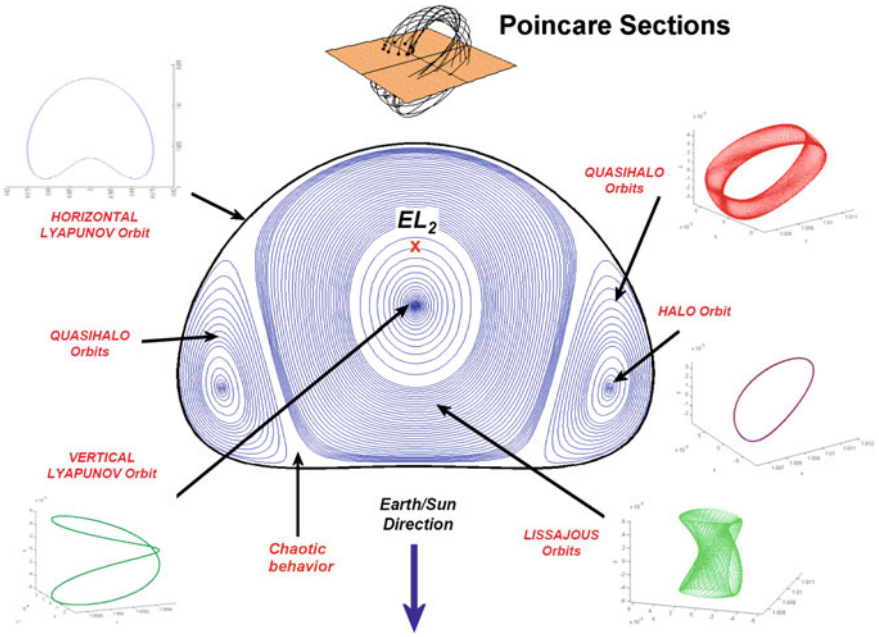

Fig. 11.22 The Poincaré maps of center manifolds orbits about a collinear libration point. *Credit* Egemen Kolemen (2012)

orbit, because the upper turning point lies closer to Earth (Fig. 11.23, middle), i.e., more on the positive side of the x-axis and its elongated part being on the Southern side. The sense of rotation as seen from Earth (minor primary) is anti-clockwise (Fig. 11.23, bottom).

Summary of Center Manifolds

Figure 11.22 gives an overview of the various periodic and quasi-periodic orbits forming the center manifolds about a collinear libration point by presenting their Poincaré maps. A Poincaré map of an orbit is the set of all points where the orbit intersects a given plane, in this case the x–y plane. This allows viewing a three-dimensional orbit in only two dimensions while preserving the essential features of the orbit.

Case Study: SOHO's Halo Orbit around EL_1 For a probe that resides in a halo orbit the SOHO mission about EL_1 is a good example (see Fig. 11.23). SOHO (Solar and Heliospheric Observatory) is an ESA/NASA space probe to study the Sun in the optical and ultraviolet spectrum at the Sun–Earth L_1 point, a.k.a. EL_1. Launched on December 2, 1995, it was planned as a 2-year mission, but mission extension lasting at least until December 2012 was approved in 2009.

From a communication point of view positioning SOHO at EL_1 would have been favorable, because there the distance to Earth is constant, as well as the S-band antenna would need merely a constant pointing to Earth. Being directly at the L_1 point, though, SOHO would be located in the line of view as seen from Earth. Therefore, the Sun radiation would jam the S-band communication. Therefore residing in this solar exclusion zone (SEZ) would render impossible any communication with Earth. The chosen Southern Class II-type halo orbit around EL_1 is a perfect solution to this problem because its extension is just large enough to circumscribe the SEZ (see Fig. 11.23, bottom) but on the other hand is small enough to require a one-dimensional antenna pointing angle of only maximal $\pm 30^\circ$ in the y-direction to Earth.

We will now draw on the SOHO mission to understand the basic physical background of its halo motion rather than just accept it as a result of the equations of motion. Let us assume that SOHO moves at position vector $\boldsymbol{\rho}$ on the halo orbit in the synodic system of the Earth rotating with ω around the Sun. SOHO's motion in the configuration plane causes in-plane Coriolis forces $\boldsymbol{F}_{Cor} = -2m(\boldsymbol{\omega} \times \dot{\boldsymbol{\rho}})$ vertical to $\boldsymbol{\rho}$. To visualize the results of this, we examine Fig. 11.23. The projection of the halo motion in the plane perpendicular to the configuration line (y–z plane) at L_1 has a component in y-direction that is perpendicular to the Sun–Earth configuration line. Let us assume this sideway motion is initially in the direction of the revolving Earth equaling the upward arrow of the SOHO orbit in the upper part of Fig. 11.23. Then this slightly increased orbit speed yields a slightly increased centrifugal force and hence a deflection in x-direction, outward toward the Earth (This is just the Coriolis effect.). According to Eq. (7.2.15) $v = \sqrt{\mu(2/r - 1/a)}$. So an increasing distance r to the Sun implies a reduction of the orbital speed until the satellite reverses its motion in y-direction. Beyond the L_1 distance its centrifugal force is smaller than needed to balance the Sun's gravitational force. The satellite therefore begins to move toward the Sun, which in turn again increases the orbital speed. This brings the satellite back to its initial point. In summary, the body has described a nearly elliptic orbit in the x–y plane. In total we therefore have a three-dimensional halo orbit: The orbit in the y–z is an ellipse and via the Coriolis forces its y-component induces in the x–y plane an orbit with an almost elliptic shape. Thus Coriolis forces are responsible for the stability of the two center-type solutions. The saddle-type solution brings about the 1-dimensional instability of a halo orbit (see next sub-section) rooted in the 1-dimensional instability of the corresponding collinear equilibrium point.

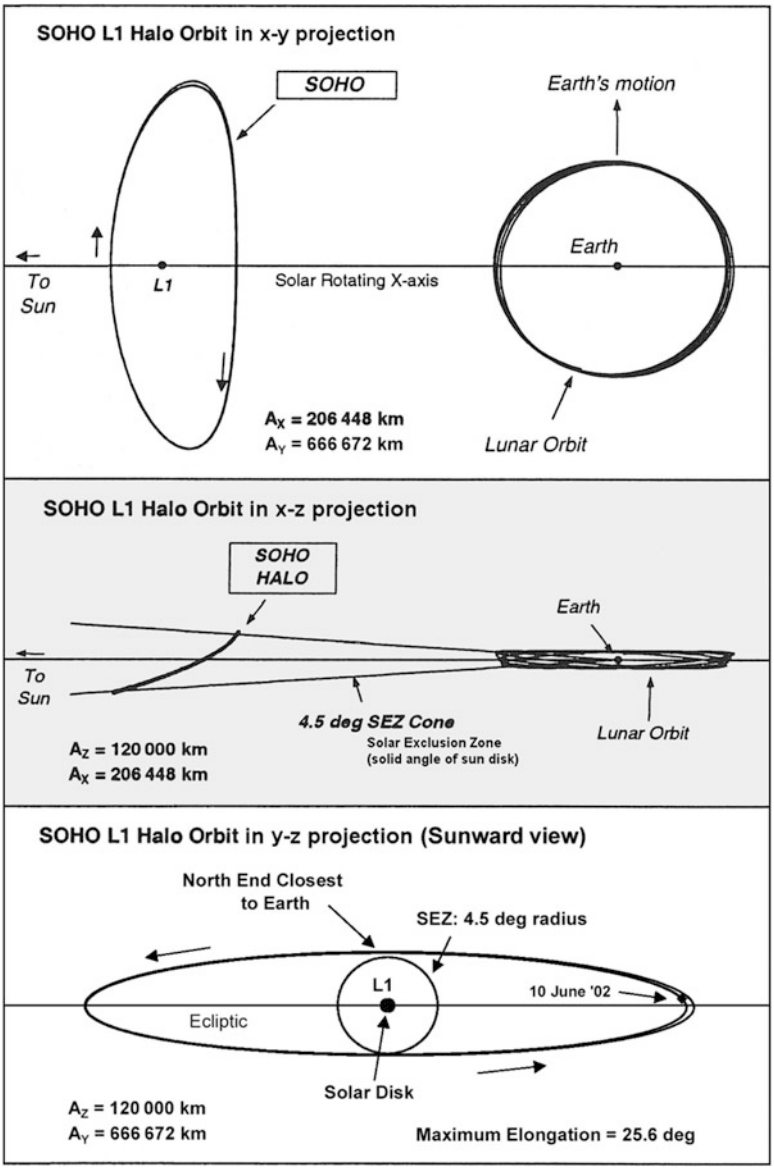

Fig. 11.23 The Southern Class II-type halo orbit of SOHO around the L_1 point in the Sun–Earth system spanning 413 × 1333 × 240 milllion m in x-, y-, and z-direction, respectively, and its projection onto the x–y plane (ecliptic plane, above), x–z plane (side view, middle), and y–z plane (sunward view, below). *Credit* ESA

For small deflection amplitudes the motions in the two perpendicular planes are not synchronous and Lissajous orbits result. For larger amplitudes $A_x \approx$ 200.000 km the increasing non-linearity of the effective potential lead to a synchronization of the two elliptic orbits, which results in a single elliptic orbit forming an certain angle with the configuration plane (see middle part of Fig. 11.23), whereby the line of nodes is the y-axis. This is the halo orbit.

Stable and Unstable Hyperbolic Manifolds

In the following explications we restrict the investigation of invariant manifolds mostly to trajectories in the x–y plane, i.e., assume that $A_z = 0$, because it already captures all their characteristics. For $A_z \neq 0$ the trajectories would exhibit just an additional independent vertical oscillation.

All the above periodic and quasiperiodic orbits of the center manifolds inherit the instability of the corresponding collinear equilibrium point (see Sect. 11.4.3). The instability is reflected in the saddle solutions $s = \pm\lambda_+$ of the linearized EoM (11.5.7) and occurs if $A_x \neq 0$. If in addition $A_1 = 0$, $A_2 \neq 0$ we have so-called **stable manifolds**, i.e., trajectories winding onto periodic center manifolds about L (see green lines in Fig. 11.25 left and right). They never truly arrive on that center manifold in finite time, but rather come asymtotically close to it as $A_2 e^{-s\tau} \to 0$. For $A_1 \neq 0$, $A_2 = 0$ we get **unstable manifolds**, i.e. trajectories winding asymptotically off center manifolds, as $A_1 e^{s\tau} \to \infty$ (see red lines in Fig. 11.25 left). Stable and unstable hyperbolic manifolds are obviously unbounded orbits.

As a specific example of hyperbolic manifolds we take those connecting to the halo orbit at the EL_1 point. For a stable manifold, i.e., a transition to that orbit, the spacecraft initially is either in a parking orbit around Earth from which a small injection burn (delta-v) will move it into the stable manifold, thus arriving at the halo orbit without any additional maneuver. Or, and quite frequently, the S/C is placed initially, as shown in Fig. 11.24, in a highly eccentric orbit about the Earth with perigee typically about 500 km and apogee at about 1.2 million km and hence at the Earth's SOI (so-called weak stability boundary, see Sect. 9.6, Fig. 9.22). In the synodic Sun–Earth system the apse line of this initial elliptic orbit rotates with the orbital period of the Earth around the Sun. The solar gravity disturbs this orbit by lifting its apogee. The extent of this perturbation strongly depends on the orientation of the apse line relative to the Sun–Earth direction. For every initial apse line orientation we thus find a different stable manifold trajectory (red lines in Fig. 11.24) onto the halo orbit at EL_1.

Transit and Non-transit Orbits

From Fig. 11.24 it is obvious that all possible stable manifold trajectories form a tube. This holds also for unstable manifold trajectories. Thus, hyperbolic manifolds geometrically are tubes, sometimes called tunnels, that partition the energy manifold and act as separatrices for the flow through the equilibrium region as shown in Fig. 11.25: Those inside the tubes transit from one side of the L region to the other and hence are called **transit orbits**, and those outside the tubes, so-called

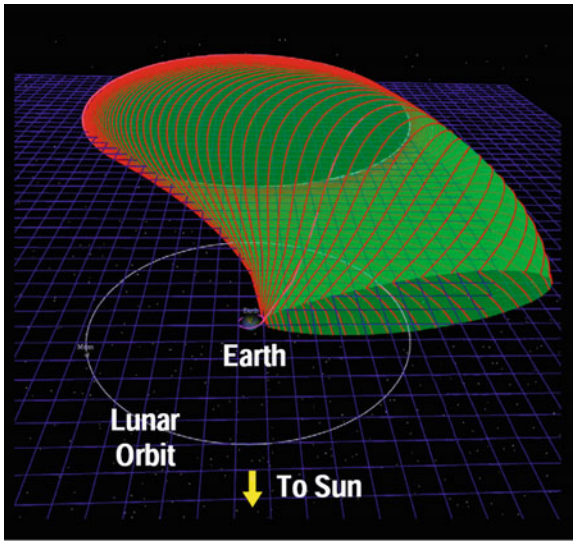

Fig. 11.24 Example of stable manifold trajectories (red lines) winding onto a halo orbit about the Sun–Earth libration point EL_2. Under the influence of the Sun's gravitational force an initially high elliptic orbit (lower end of tube) with perigee at about 500 km and apogee at about 1.2 million km will undergo a transition onto the halo orbit. The concrete trajectory depends on the slightly different initial conditions of the initial orbit. *Credit* Martin W. Lo (2001)

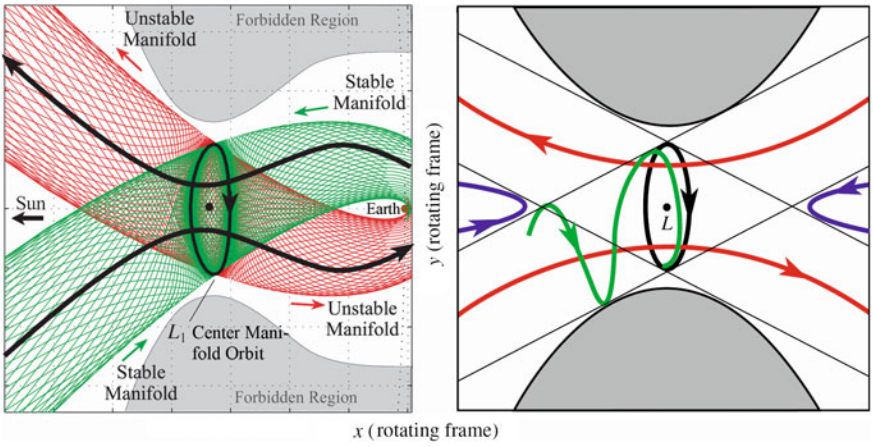

Fig. 11.25 Left: Shown are the projections of trajectories of the stable manifold (green) onto, and unstable manifold trajectories (red) off a center manifold orbit about EL_1. Right: Unbounded orbits in the vicinity of a L region. Shown are transit orbits (red), non-transit orbits (blue) and a trajectory of a stable manifold (green). The parallel lines delineate the manifold tubes. In the left picture the black arrows indicate smooth transit orbits. *Credit* Fig. 11.25 left, Martin W. Lo (2001); Fig. 11.25 right, reproduced from Koon (2000) with the permission of AIP Publishing

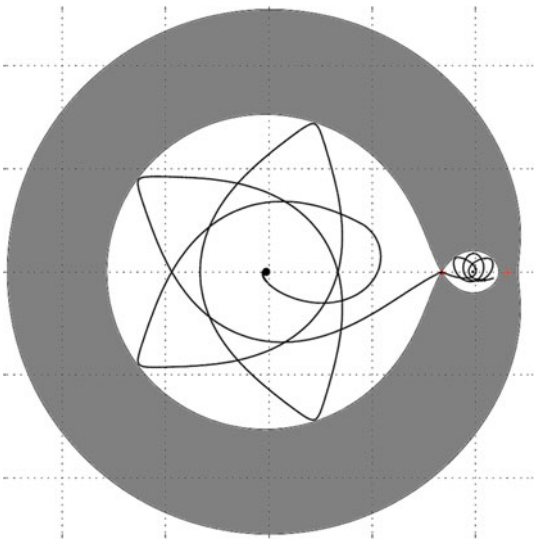

Fig. 11.26 Example for an L_1 transit Earth–Moon in the synodic reference frame

non-transit orbits, are reflected from the L region. If even $A_x = 0$, we get stable transit and non-transit orbit that smoothly transit the L region (see Fig. 11.25 right) or are smoothly reflected from it.

As an interesting example, Fig. 11.26 shows an Earth–Moon transit orbit at L_1 with a ballistic capture at the Moon. Since $v \approx 0$ at L_1, the trajectory has $A_x \approx 0$ at that point, meaning a smooth transition from the inner region to the Moon-bound region.

Once in the center manifold orbit, a small thrust (kick-burn) will bring the S/C into an unstable manifold drifting away from EL_2. The tubes of stable and unstable manifolds passing through the center manifold orbit about EL_1 are shown on the left side of Fig. 11.25.

Because all center manifolds inherit the instability of the corresponding collinear equilibrium point, some minor station-keeping effort is always required, which typically is of the order of 50 cm/s per year.

Heteroclinic and Homoclinic Orbits

Of course, similar windings exist onto and off center manifold orbits at EL_2. Therefore, there exist commuting orbits, as shown in Fig. 11.27, that transit on an unstable manifold out of a center manifold orbit about L_1, transverse Earth's region via a so-called heteroclinic (meaning "connecting") orbit, and converge on a stable manifold into a center manifold orbit about L_2—and back again. Such trajectories around the major primary that convey halo orbits from one libration point to another

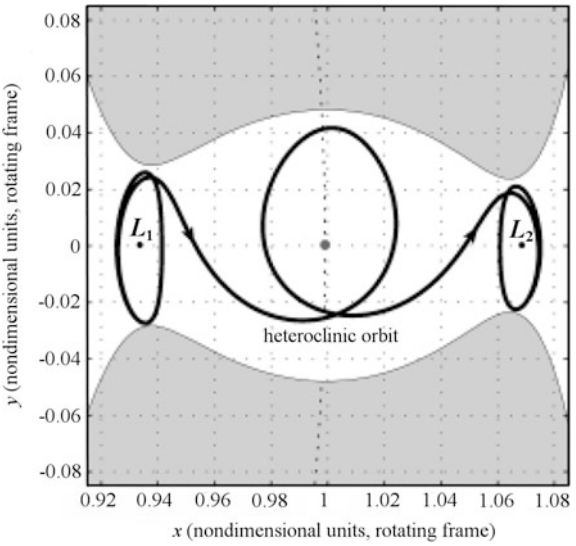

Fig. 11.27 A heteroclinic orbit connecting center manifold orbits at EL_1 and EL_2 via a stable and unstable manifold orbit. Reproduced from Koon (2000) with the permission of AIP Publishing

are called **heteroclinic orbits**. On the other hand, trajectories that wind off a Class I-type halo orbit, circle around the major primary, and wind onto a Class II-type halo orbit (or vice versa, see above) about the *same* libration point, i.e., which just change the sense of rotation in an halo orbit, are called **homoclinic orbits**.

Case Study: Genesis Mission to the Halo Orbit about EL_1 An interesting case in point was the Genesis mission where the invariant manifolds were utilized for a nearly powerless mission to and from the EL_1 point. The Genesis probe was launched on August 8, 2001, with the mission objective to collect a sample of solar wind atomic particles at EL_1 and return it to Earth for analysis. After about 3 years it returned to Earth where it unfortunately crashed into the desert floor due to a design flaw in a deceleration sensor, which should have triggered the parachute deployment. Figure 11.28 depicts the Genesis mission trajectory into a "halo orbit" (actually a Lissajous orbit) about EL_1 and then via a heteroclinic orbit into a near halo orbit at EL_3 to adjust for a daylight reentry into Earth's atmosphere.

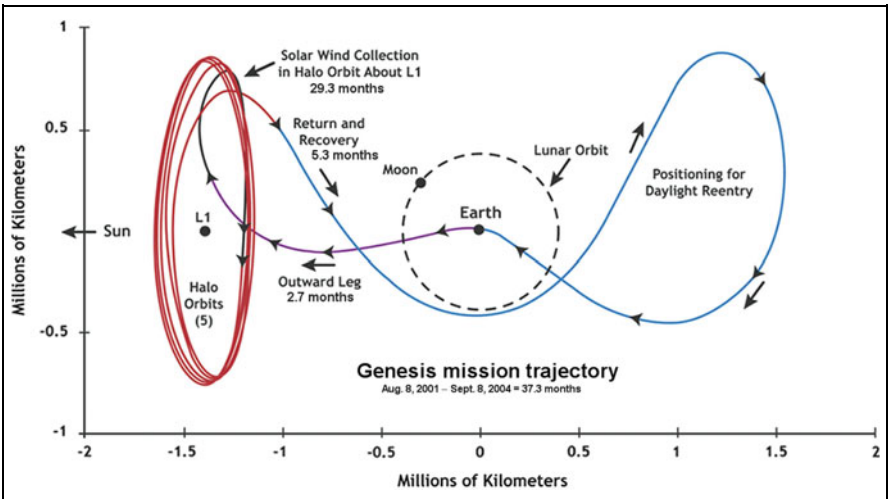

Fig. 11.28 The Genesis mission trajectory projected onto the x–y plane. *Credit* NASA

11.5.3 Equilateral Libration Points

We now consider the detailed dynamics in the vicinity of equilateral libration points L_4, L_5.

Equation of Motion Near Equilateral Libration Points

By the same token as in Sect. 11.5.2 we want to study the dynamics in the vicinity of the equilateral libration points and evaluate the right-hand side of Eq. (11.5.4) in powers of r. We therefore expand the expression for the distances to the equilateral libration points

$$\Delta r_i = \sqrt{(x - x_i)^2 + (y - y_i)^2 + z^2} = \sqrt{x_i^2 + y_i^2 - 2(x_i x + y_i y) + u^2}$$

with $u = \sqrt{x^2 + y^2 + z^2}$. According to Table 11.2 for equilateral libration points holds $x_i^2 + y_i^2 = (\mp 1/2)^2 + \left(\pm\sqrt{3}/2\right)^2 = 1$. Identifying $\alpha_i \equiv (x_i x + y_i y)/u$ the expansion reads

$$\frac{1}{\Delta r_i} = \frac{1}{\sqrt{1 - 2\alpha_i u + u^2}} = 1 + \sum_{n=1}^{\infty} u^n P_n(\alpha_i)$$

The equation of motion (11.5.4) then reads

$$\begin{pmatrix} x'' - 2y' - x \\ y'' + 2x' - y \\ z'' \end{pmatrix} = \boldsymbol{\rho}_L + \frac{\partial}{\partial \boldsymbol{r}} \left(\frac{1-\mu}{\Delta r_1} + \frac{\mu}{\Delta r_2} \right)$$
$$= \boldsymbol{\rho}_L + \frac{\partial}{\partial \boldsymbol{r}} \sum_{n=1}^{\infty} u^n \left[(1-\mu) P_n \left(\frac{x_1 x + y_1 y}{u} \right) + \mu P_n \left(\frac{x_2 x + y_2 y}{u} \right) \right]$$

For $n = 1$ $P_1(\alpha) = \alpha$ and considering Table 11.2 we have

$$\frac{\partial}{\partial \boldsymbol{r}} [(1-\mu)(x_1 x + y_1 y) + \mu(x_2 x + y_2 y)]$$
$$= \begin{pmatrix} (1-\mu)x_1 + \mu x_2 \\ (1-\mu)y_1 + \mu y_2 \\ 0 \end{pmatrix} = \begin{pmatrix} -0.5 + \mu \\ \mp\sqrt{3}/2 \\ 0 \end{pmatrix} = -\boldsymbol{\rho}_L$$

When calculating also the term with $n = 2$ (exercise) we get

$$\begin{aligned} &x'' - 2y' - \frac{3}{4}x \mp \frac{3\sqrt{3}}{4}(1-2\mu)y = 0 \\ &y'' + 2x' - \frac{9}{4}y \mp \frac{3\sqrt{3}}{4}(1-2\mu)y = 0 \\ &z'' + z = 0 \end{aligned} \qquad \textbf{EoM near } \boldsymbol{L_4, L_5} \qquad (11.5.9)$$

These are the linearized equations of motion in the vicinity of the two equilateral libration points, whereby the upper minus sign applies for L_4 and the lower plus sign for L_5. We recall that in literature L_4 and L_5 might be labeled inversely.

Invariant Manifolds Near Equilateral Libration Points

Upon solving these equations of motion we realize that as in the collinear equilibrium case the third equation is decoupled and describes a harmonic oscillator about the x–y plane, with frequency $\omega_z = n = \sqrt{G(m_1 + m_2)/d^3} = 2\pi/T$ i.e., in step with the synodic revolution frequency. For the two coupled equations we again make the standard ansatz $x = x_0 \exp(\lambda\tau)$, $y = y_0 \exp(\lambda\tau)$ and find for the characteristic polynomial

$$\lambda^4 + \lambda^2 + \frac{27}{4}\mu(1-\mu) = 0$$

of the differential equation matrix

$$\boldsymbol{A} = \begin{pmatrix} 0 & 0 & 1 & 0 \\ 0 & 0 & 0 & 1 \\ 3/4 & c & 0 & 2 \\ c & 9/4 & -2 & 0 \end{pmatrix}$$

which satisfies $\boldsymbol{X}' = \boldsymbol{A}\boldsymbol{X}$, where $\boldsymbol{X} = (x, y, x', y')$, with $c = \pm 3\sqrt{3}(1-2\mu)/4$, where the upper plus sign is for the L_4 point and the lower minus sign is for the L_5 point. Considered as a quadratic characteristic equation for λ^2 the terms in the characteristic equation do not exhibit any sign changes. According to Descartes' rule of signs this implies that there are no positive roots and hence only two negative roots, $\lambda_{1,2}^2 < 0$. By defining $\omega_{1,2} = \sqrt{-\lambda_{1,2}^2}$ we get

$$\omega_{1,2} = \frac{n}{\sqrt{2}}\sqrt{1 \pm \sqrt{1 - 27\mu(1-\mu)}} \tag{11.5.10}$$

with $n = \sqrt{G(m_1 + m_2)/d^3} = 2\pi/T$ the orbital frequency of the synodic system. Because the solutions of the characteristic polynomial are all imaginary the general solutions of the linearized EoM (11.5.9) can be generally written as (see also Murray and Dermott (1999) or Roy (2005))

$$\begin{aligned} x(t) &= \alpha_0 + \alpha_1 \sin(\omega_1 t + \varphi) + \alpha_2 \sin(\omega_2 t + \varphi) \\ y(t) &= \beta_0 + \beta_1 \cos(\omega_1 t + \phi) + \beta_2 \cos(\omega_2 t + \phi) \end{aligned} \tag{11.5.11}$$

From this we recognize that $\omega_{1,2}$ are the angular frequencies of two modes, $i = 1, 2$, with amplitudes α_i, β_i and phases φ, ϕ, which are determined from the initial conditions. As in the case of the collinear equilibrium the amplitudes are coupled via $\omega_{1,2}$ and the curvature of the potential mirrored by c, reducing the number of free parameters to be determined by the initial conditions to four. The two modes are periodic motions about the equilateral libration points, if and only if both angular frequencies are truly real. This is the case if in Eq. (11.5.10) the radicand $1 - 27\mu(1-\mu) \geq 0$, implying $\mu \leq \left(27 - 3\sqrt{69}\right)/54 = 0.0385$, in turn implying

$$m_1 \geq \frac{25 + 3\sqrt{69}}{2} m_2 = 24.96\, m_2 \tag{11.5.12}$$

This condition corresponds to a minimal curvature of the effective potential at the equilateral libration points, which is necessary to cause enough acceleration and hence speed and Coriolis force to curve the body on a bounded periodic orbit. As all the Sun–planet and planet–Moon constellations in our solar system fulfill condition Eq. (11.5.12), all equilateral libration points in our solar system are dynamically stable. This is true even for the Earth–Moon system where $m_{Earth} = 81.30094\, m_{Moon}$. Actually, as of January 2011, 4790 asteroids, so-called Trojans, were found at the equilateral libration points of the Sun–Jupiter (4779), Sun–Mars (4) and Sun–Neptune (7) systems. The first discovered and most famous is Achilles, which moves in a bounded orbit about Jupiter's L_4 point.

How do these two periodic modes look like? Because $\mu \ll 1$, we can approximate Eq. (11.5.10) to

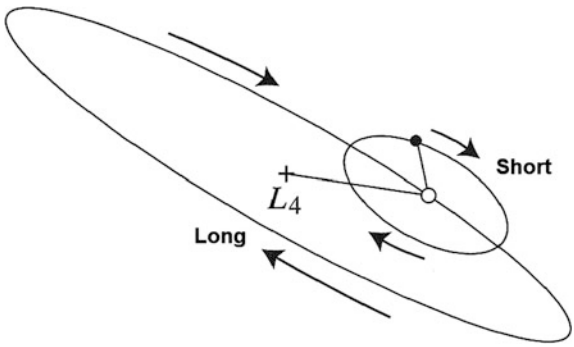

Fig. 11.29 The epicyclic orbit of a body (full dot) around L_4, which may be considered as motion on a short-term ellipse, the center of which (open dot) in turn moves on a long-term ellipse around L_4. *Credit* Murray and Dermott (1999)

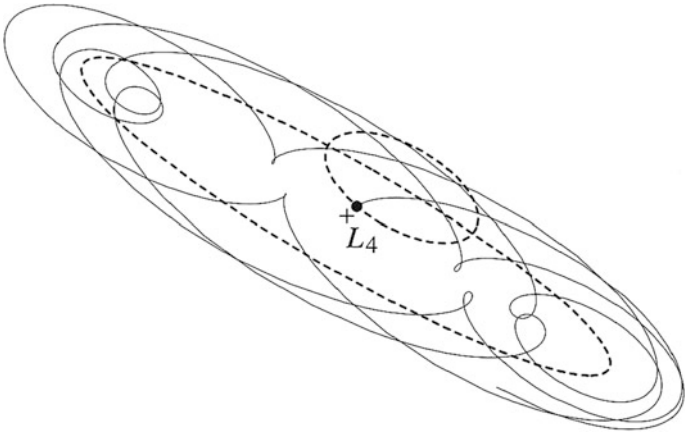

Fig. 11.30 The epicyclic motion (full line) of a body with Jacobi constant $C = -1.563$ around the equilateral libration point L_4 in the Earth–Moon system, as a composite of the two basic modes (dashed line) over 13 orbital periods. *Credit* Murray and Dermott (1999)

$$\omega_1 = n\left(1 - \frac{27}{8}\mu\right) \approx n$$
$$\omega_2 = n\sqrt{\frac{27}{4}\mu}$$

Hence there is one short-term mode with period $2\pi/\omega_1 \approx T$ and semi-major axis α_1, β_1 and a long-term mode with period $2\pi/\omega_2 = T\sqrt{4/(27\mu)}$ and semi-major axis α_2, β_2. The total movement can be considered as a short-term elliptic epicycle with semi-axis ratio $\alpha_1/\beta_1 = \sqrt{3\mu}$, moving on a long-term ellipse with semi-axis ratio $\alpha_2/\beta_2 = 1/2$ around the equilateral libration point (see Fig. 11.29). This composite motion is displayed in Fig. 11.30. The trajectory may (but does not

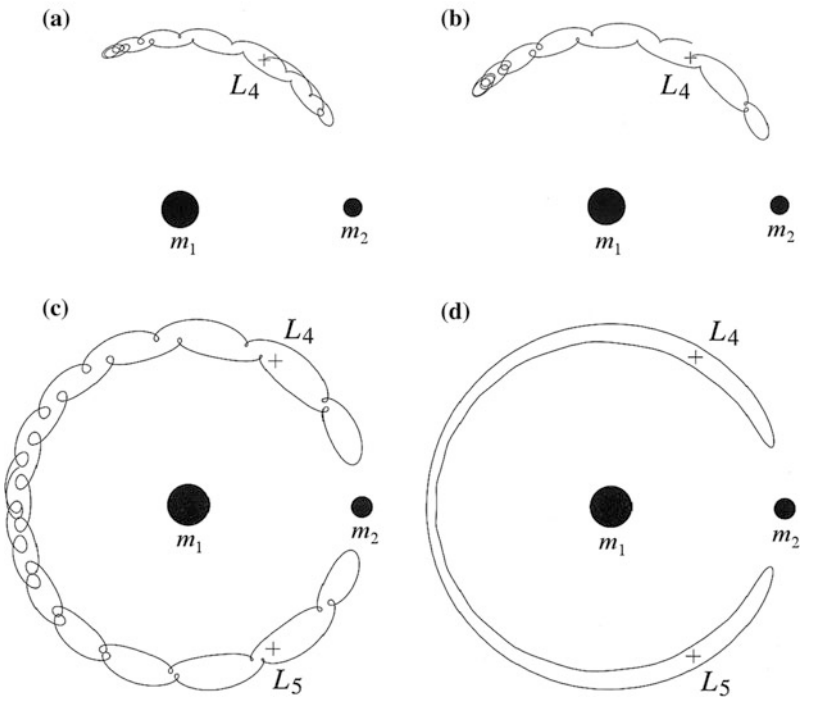

Fig. 11.31 Librations about L_4/L_5 points in the synodic frame with varied initial conditions (see text): (a and b) tadpole orbits over 13 synodic periods for $\mu = 0.001$ matching almost the Sun–Jupiter system; and (c and d) horseshoe orbits for $\mu = 9.53875 \times 10^{-4}$ equaling the Sun–Jupiter system. *Credit* Murray and Dermott (1999)

have to) touch the zero-velocity curve at some points with zero velocity, but cannot cross it. The smaller the excluded Hill zone around the equilateral libration point, the closer is the trajectory around the equilateral libration point.

In summary, bounded periodic orbits affected by Coriolis forces exist both about collinear and equilateral libration points. In physics a periodic motion around a equilibrium point is denoted as "libration", the term "libration points" just stems from the existence of such periodic orbits around these points.

Tadpole and Horseshoe Orbits

The epicyclic motion described above occurs only if it does not deviate too far from the equilateral libration point. How does an orbit look like if its excursions become bigger? In this case approximate analytical solutions cannot be provided any more. But numerical solutions of the EoM (11.4.10) show that orbits with decreasing orbital energies and increasingly initial tangential velocities become more and more elongated. Figure 11.31a, b depictures the trajectories of a body starting in Fig. 11.31a

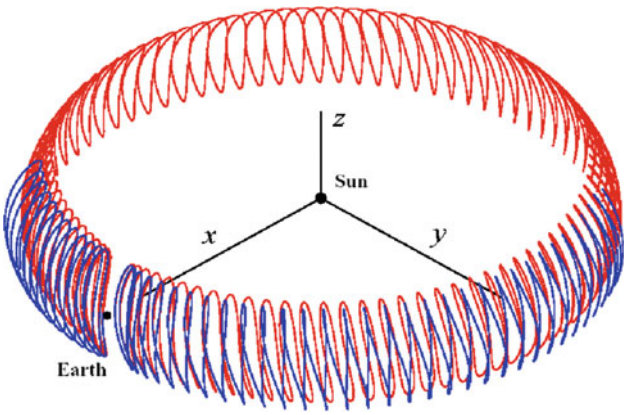

Fig. 11.32 Three-dimensional representation of the horseshoe orbit of asteroid 2002 AA29 in the synodic Sun–Earth system. The looping is caused by a finite value of the z-component of the initial velocity. The blue trajectory is the horseshoe orbit after reversal at the end points of the horseshoe. *Credit* M. Connors, Athabasca University, and © Wiley

with $\dot{\boldsymbol{\rho}}_0 = 0$ at $\boldsymbol{\rho}_0 = (\xi_{L4} + 0.0065,\ \eta_{L4} + 0.0065,\ 0)$ and in Fig. 11.31b with $\dot{\boldsymbol{\rho}}_0 = 0$ at $\boldsymbol{\rho}_0 = (\xi_{L4} + 0.008,\ \eta_{L4} + 0.008,\ 0)$, i.e., close to L_4 with $C \approx -\Omega_{L4}$. Because they depart fairly far from the equilibrium points and owing to their shape they are called *tadpole orbits*. While the short-term mode of motion is preserved, the semi-major axis of the long-term ellipses stretches to a circular arc along the circular orbit of m_2. If the Jacobi constant is decreased and/or increasing initial velocity is more tangential the tadpole orbits elongates and arcs until both meet at the L_3 point and then merge: A so-called *horseshoe orbit* has formed as depicted Fig. 11.31c for $\dot{\boldsymbol{\rho}}_0 = (0,\ -0.06118,\ 0)$ at $\boldsymbol{\rho}_0 = (\xi_{L3} + 0.02372,\ 0,\ 0)$, i.e., close to L_3. For suitable initial tangential velocities the amplitude of the short-term mode can be suppressed forming a smooth horseshoe orbit as shown in Fig. 11.31d for $\dot{\boldsymbol{\rho}}_0 = (0,\ -0.04032,\ 0)$ at $\boldsymbol{\rho}_0 = (\xi_{L3} - 0.02705,\ 0,\ 0)$. In this case the object moves with a nearly constant velocity on an equipotential line in the system of the two primaries (see e.g., Fig. 11.11), which encompasses the L_3, L_4, and L_5 points. If the initial condition is such that the suitable tangential velocity has a component in z-direction that is out of the configuration plane then vertically looping horseshoe orbits occur as depicted in Fig. 11.32.

All Jupiter and Mars Trojans known so far move on tadpole orbits. But only recently the asteroids 3753 Cruithne, 2002 AA29, and 2010 SO16 were found in the Sun–Earth system as three examples of horseshoe orbits. However, 3753 Cruithne moves on a horseshoe orbit with a high eccentricity, $e = 0.515$, and high inclination, $i = 19.81°$, to the ecliptic, which is why it is sometimes not counted as a horseshoe object. In addition, in 1980 Voyager 1 found the two equally massive asteroids Janus and Epimetheus with identical orbital radii around Saturn, which move on horseshoe orbits relative to each other. Trojans on tadpole orbits, asteroids on horseshoe orbits,

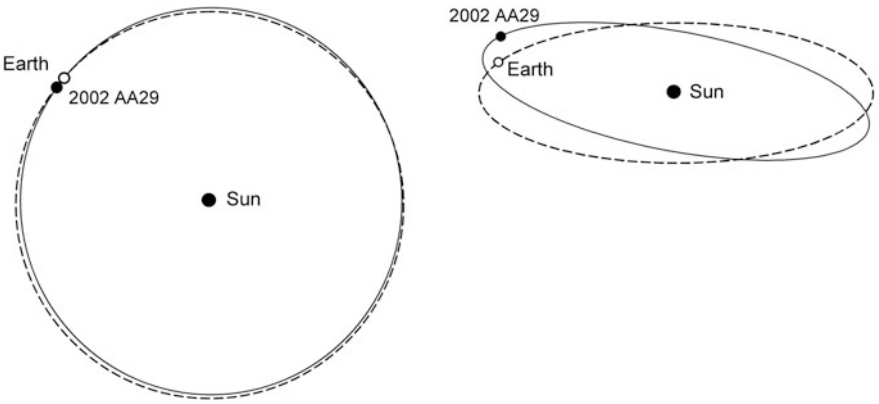

Fig. 11.33 The orbit of asteroid 2002 AA29 in the heliocentric system in the ecliptic (left) and viewed oblique (above)

and so-called quasi-satellites are called **co-orbital objects**, because they move in the same or nearly the same orbit of a celestial body around a central body.

With all these complex co-orbital objects it should be remembered that in the inertial barycentric system of the primaries the test mass always moves on elliptic orbits around the barycenter, which deviate just slightly from the minor primary. Only the transition into the synodic system results in the complex relative motions just discussed. In this way the horseshoe orbit from Fig. 11.32 corresponds to the full elliptic orbits in the inertial heliocentric system in Fig. 11.33.

11.6 Problems

Problem 11.1 *Alternative Proof of Sundman's Inequality*
Alternatively to Sect. 11.1.2 prove Sundman's inequality Eq. (11.1.4)

$$E_{kin} \geq \frac{L^2}{2I}$$

by looking for the minimum of

$$E_{kin,\theta} = \frac{1}{2}\sum_i m_i v_{i,\theta}^2 \leq \frac{1}{2}\sum_i m_i \left(v_{i,\theta}^2 + v_{i,r}^2\right) = E_{kin}$$

with respect to the angular momentum of each body.

Problem 11.2 *Collinear Configuration*
Let Eqs. (11.2.1) and (11.2.2) be given. Prove that α is the unequivocal *positive* root of $\mu_3 = \alpha^3 \mu_2$.

Hint: cf. Guthmann (2000, pp. 242ff)

Problem 11.3 *Circularly Rotating Collinear Configuration*
Show that for a circularly rotating collinear configuration the orbital period is

$$T = 2\pi\sqrt{\frac{x_{12}^3}{\mu}\frac{m_1' - m_3'\chi}{m_1'\chi^2 - m_3'}} \quad \text{with } \mu = GM = G\left(m_1' + m_2' + m_3'\right)$$

Hint: Starting from the center of mass equation $m_1'x_1 + m_2'x_2 + m_3'x_3 = 0$ show that

$$x_2 = x_{12}\frac{m_1' - m_3'\chi}{M}$$

and finally because of $n^2 = \mu_i/x_i^3$ the wanted result.

Problem 11.4 *Circularly Rotating Equilateral Configuration (hard)*
Show that for a circularly rotating equilateral configuration $\Delta r = r_{12} = r_{23} = r_{13} = const$ Eq. (11.2.11)

$$n = \frac{2\pi}{T} = \sqrt{\frac{\mu_i}{r_i^3}} = \sqrt{\frac{\mu}{(\Delta r)^3}}$$

holds.

Hint: First show $n = \sqrt{\mu_i/r_i^3}$, and then $\mu_i/r_i^3 = \mu/(\Delta r)^3$ by using the center of mass equation $m_1\boldsymbol{r}_1 + m_2\boldsymbol{r}_2 + m_3\boldsymbol{r}_3 = 0$.

Problem 11.5 *Collinear Libration Points (tedious but good practice)*
(a) For the L_3—point the condition equation for Δ_3 is Eq. (11.3.4). By making the ansatz $\Delta_3 = 1 + a\mu + c\mu^3$ and assuming that the term of order $b\mu^2 = 0$, prove that

$$a = -\frac{7}{12}, \quad c = -\frac{12103}{13824}$$

(b) For L_1 and L_2 points make the ansatz $\Delta_i = 1 + a_i\lambda + b_i\lambda^2 + c_i\lambda^3$ with $\lambda = (\mu/3)^{1/3}$ and show that by inserting into the according condition Eqs. (11.3.5) and (11.3.6) one gets $a_1 = -a_2 = -1$, $b_1 = b_2 = 1/3$, and $c_1 = -c_2 = 1/9$.

Problem 11.6 *Jacobi Constant Approximations*
By applying Eq. (11.3.7), show that for the Jacobi constant of a stationary test mass in the synodic system at the libration points the following power series expansions up to order $O(\mu)$ hold

$$C_{L1} = -\frac{3}{2} - \frac{3}{2}\lambda + 5\lambda^3 + \ldots$$
$$C_{L2} = -\frac{3}{2} - \frac{3}{2}\lambda + 7\lambda^3 + \ldots$$
$$C_{L3} = -\frac{3}{2} - \frac{3}{2}\lambda^3 + \ldots$$
$$C_{L4} = C_{L5} = -\frac{3}{2} + \frac{3}{2}\lambda^3 + \ldots$$

with

$$\lambda = \left(\frac{\mu}{3}\right)^{1/3}, \quad \mu = \frac{m_2}{m_1 + m_2}$$

Hint: Consider Eq. (11.4.9) for $v = 0$.